UNIVERSITY OF CALIFORNIA, SAN DIEGO

High-throughput piezoelectric-actuated micro-fluorescence-activated cell sorter (μFACS)

A dissertation submitted in partial satisfaction of

the requirements for the degree Doctor of Philosophy

in

Bioengineering

by

Chun-Hao (Randy) Chen

Committee in charge:

Professor Xiao-Hua Huang, Chair
Professor Yu-Hwa Lo, Co-Chair
Professor Pao Chau
Professor Michael Heller
Professor Kun Zhang

The dissertation of Chun-Hao (Randy) Chen is approved, and it is acceptable in quality and form for publication on microfilm and electronically:

_____

_____

_____

_____

Co-Chair

_____

Chair

University of California, San Diego

2010

Dedication

This dissertation is dedicated to my family.

Table of Contents

List of Figures

List of Tables

Acknowledgements

Throughout my Ph.D study at UCSD, I have met many fascinating mentors, labmates, friends, and collaborators who have given me tremendous support that helped, nurtured, and guided me to become a better researcher and a more mature person. First, I would like to thank my advisor, Prof. Yu-Hwa Lo for his support and faith in me. As a research advisor, he has always been there to offer guidance whenever I have any technical questions or encounter any roadblocks in research. Also, he has always shown great patience and caring toward me both inside and outside of laboratory. I am very grateful to have him as my advisor. I also want to thank my other members of dissertation committee, Prof. Xiao-Hua Huang, Prof. Kun Zhang, Prof. Michael Heller, and Prof. Pao Chau. Their advices toward my research studies have been invaluable and have helped me overcoming many technical challenges.

I would also like to thank my labmates: Victor Lien, Eugene Berdichevsky, Nicole Justis, Jessica Godin, Sung Hwan Cho, Frank Tsai, Wen Qiao, Kai Zhao, Ashkan Arianpour, and Shawn Meade. Secrets to technical breakthroughs mostly come from little tricks during fabrication, implementation, and experimentation and many of the research successes in this thesis are mainly resulted from the skills they have passed down to me. Beside academic life, they have shown and guided me to mature in my personal life, and I feel very lucky and grateful to have them in this period of my life. In addition, I want to thank my collaborators: Sam Chang, Jeff Gole, Wenjin Cui, Dmitri Simberg. The thesis, especially chapter 6, could not have been easily done without their generous assistance. Through interactions with them, they have broadened my research

scope and vision. Also, I want to thank several UCSD fellow graduate students and postdocs: Ian Liang, Dayu Teng, Fred Lo, and Ann Shih.

Last but not least, I want to thank my loving parents and siblings, A-Wen Lin, Kun-Hsin Chen, Calvin Chen, and Ruby Chen for they have cared for me with unconditional love. Words cannot fully express the gratitude and the love I feel for them. My best friend, Harry Choi, who have gone through up and downs in life with me and I feel grateful and fortunate having him by my side. Lastly, my fiancé, Sherry Yeh, has constantly shown unbelievable patience and love toward me regardless of what situation and emotional state I am in.

Chapter 1 or portion thereof has been published in ***Tay & Francis Group*****, Handbook of Optofluidics, ch. 19 (2010)**. Chapter 2 or portion thereof has been published in ***IEEE Photonics Technology Letter,*** **vol. 19, Iss. 6, pp. 441~443 (2007). Chapter 4** or portion thereof has been published in ***Biomedical Microdevice,*** **Vol. 11, Iss. 6, pp. 1223-1231** and ***Lab Chip*****, Vol. 10, pp. 1567-1573.** Chapter 5 or portion thereof has been published in ***Biomedical Microdevice,*** **Vol. 11, Iss. 6, pp. 1223-1231** and ***Lab Chip*****, Vol. 10, pp. 1567-1573.**

Vita

December, 2003	Bachelor of Science in Mechanical Engineering University of California, Berkeley
December, 2003	Bachelor of Science in Economics University of California, Berkeley
2004-2010	Graduate Student Researcher Department of Bioengineering University of California, San Diego
December, 2010	Doctor of Philosophy in Bioengineering University of California, San Diego

Publications

1. **Chun Hao Chen**, Sung Hwan Cho, Sam Chang, Frank Tsai, Kun Zhang, and Yu-Hwa Lo. "An integrated μFACS technology combined with Tyramide Signal Amplification enhanced Fluorescence in situ Hybridization (TSA-FISH) for isolation of rare bacteria and removal of cell-free DNA." Manuscript in preparation

2. Sung Hwan Cho*, **Chun-Hao Chen***, Frank Tsai, Jessicca Godin, and Yu-Hwa Lo. "Human mammalian cell sorting using a highly integrated micro-fabricated fluorescence-activated cell sorter (μFACS)." **Lab Chip** 10, 1567-1573 (2010) ***Both authors contribute equally.**

3. **Chun-Hao Chen**, Sung Hwan Cho, Frank S. Tsai, Ahmet Erten, and Yu-Hwa Lo, "Microfluidic cell sorter with integrated piezoelectric actuator," ***Biomedical Microdevices***, Vol. 11, pp. 1223-1231 Aug. 2009.

4. Jessica Godin, **Chun-Hao Chen**, Sung Hwan Cho, Wen Qiao, Frank S. Tsai, Yu-Hwa Lo, "Microfluidics and photonics for Bio-System-on-a-Chip: A review of advancements in technology towards a microfluidic flow cytometry chip" ***Journal of Biophotonics***, Vol. 1, Iss. 5, pp. 355~376 (2008). (***review*** paper).

5. **Chun-Hao Chen**, Frank Tsai, Victor Lien, Nicole Justis, and Yu-Hwa Lo, "Scattering-Based Cytometric Detection Using Integrated Arrayed Waveguides with Microfluidics," ***IEEE Photonics Technology Letters***, Volume 19, Issue 6, pp. 441~443, March 2007.

6. Sung Hwan Cho, **Chun Hao Chen**, Frank S. Tsai, and Yu-Hwa Lo, "Automated Real-time sorting with high throughput microfabricated fluorescence-activated cell sorter," ***IEEE EMBC***, Minneapolils, MN, Sep. 2009.

7. Chen, C. H., S. H. Cho, A. Erten, and Y.-H. Lo (2008) "High-Throughput Cell Sorter with Piezoelectric Actuation." Proceedings of 12th International MicroTAS Conference, San Diego, USA

8. Sung Hwan Cho, Jessica Godin, **Chun Hao Chen**, Frank S. Tsai, Yu-Hwa Lo, "Microfluidic Photonic Integrated Circuits," ***SPIE APOC***, Oct. 2008. ***(invited)***

9. **Chun H. Chen**, Frank Tsai, and Yu-Hwa Lo, "High-Sensitivity scattering-based detection under symmetrical arrayed-waveguide platform," ***IEEE LEOS***, Montreal, Quebec, Canada, July 2006.

ABSTRACT OF THE DISSERTATION

High-throughput piezoelectric-actuated micro-fluorescence-activated cell sorter (μFACS)

by

Chun-Hao (Randy) Chen

Doctor of Philosophy in Bioengineering

University of California, San Diego, 2010

Professor Xiao-Hwa Huang, Chair
Professor Yu-Hwa Lo, Co-Chair

In this thesis, I have developed a piezoelectric-actuated micro-fluorescence-activated cell sorter (μFACS) and demonstrate its performances using various biological samples including mammalian cell and bacteria. Three major developments in this work included a high-sensitivity detection system, fast-response on-chip piezoelectric cell sorting module, and system integration. In my early work, optical arrayed waveguides combined with cross-correlation signal processing algorithm are implemented to achieve high-sensitivity scattering detection. The insight gained from the algorithm further allowed me to design and implement a spatial-filter based (space-time coding)

fluorescent detection system. The system enables not only signal amplification (~ 18 dB SNR enhancement) but also sorting even verification, allowing real-time optimization of sorting parameters. The first generation on-chip cell-sorting module involves flow-redirection using the principle of nozzle-diffuser, but due to the periodic flow and high fluid disturbance resulted from high-voltage piezoelectric actuation, the sorting module was redesigned, resulting in piezoelectric-actuated cell sorting module. The inexpensive module was able to manipulate single cells at high rate (> 1000 cells/s) under low powered actuation (< 10 mW and < 10 V_{p-p}).

Integration of detection and sorting systems is achieved through the implementation of the preprogrammed FPGA-embedded external driver enables closed-loop control for triggering fluorescence-activated cell sorting. With the sorting event verification capability, sorting efficiency was found to be > 80%. Sample enriching experiments were done using beads and human mammalian cells, showing an enrichment factor > 200 fold (comparable to commercial FACS), which is the higest among μFACS systems.

The developed integrated μFACS was also applied to address the challenges (detection sensitivity and cell-free DNA contamination) commonly encountered in single-cell genome sequencing. Flow cytometry-modified Tyramide Signal Amplification Fluorescence in situ Hybridization (TSA-FISH) and two-step optofluidic light confinement were implemented to enhance sensitivity. Also, dual-round cell-free DNA purification was performed and compared to commercial FACS, showing comparable results. Sorting of rare bacteria was achieved, showing 223-fold enrichment.

I hope the work sets the benchmark for the future development of μFACS systems. I believe the realization of a truly hand-held μFACS that can be afforded by every research labs and clinics is not far off.

Chapter 1

Introduction and background

Flow cytometry, a concept originated back in 1934 by Moldavan [1], has evolved to become an indispensable bioanalysis tool in the biological community. Due to the significant technological advancement in the development of flow cytometers, researchers are able to study and characterize the physical (cell size, shape, and granularity) and biochemical (DNA content, cell cycle distribution, and viability) properties of cells in a highly quantitative manner. A state-of-the-art flow cytometer

(also known as a fluorescence-activated cell sorter, or FACS) can interrogate and sort cells with a throughput of tens of thousands of cells per second, making possible rare-event studies, such as the identification of bacterial cells [2] or the isolation of stem cells [3]. Currently, more than 30,000 flow cytometers have been employed in various research institutions and hospitals [4], and the demand has been growing. However, current FACS machines (especially ones with sorting capabilities) are bulky (~ 400 lb), expensive (~$500k), and require specially trained personell for operation and maintenance, making the machines inaccessible to most mid-sized hospitals, clinics, and research labs not to mention hospitals in resource-poor countries. Also, in biological community, there is a growing interest in single-cell analysis because researchers have now realized that the measurement of cellular activities in bulk (i.e. 10^3-10^6 cells) could yield results which are completely different from single-cell analysis (such as in gene expression studies and cellular response to external stimuli). Therefore, to accelerate research progress (e.g. basic research, clinical studies, and biotechnological developments), it is desirable to find an alternative cell-sorting platform which can provide significant cost and size reduction while maintaining comparable operation performances.

In recent development, to address the aforementioned limitations, microfluidic (or lab-on-a-chip) platforms have been extensively studied [5] and exploited for various biological applications due to the benefits they offered such as the ease of integration, size reduction, and small reagent usage. Therefore, in this disseration, I will demonstrate a microfluidic microfabricated fluorescecence-activated cell sorter

(μFACS) that integrate photonics (optical wavegudes), acoustics (piezoelectric actuation), spatial-filtered based light collection system in conjunction with a real-time electronics control system to achieve superior performances at a fraction of the cost and size of the commercial FACS machines. In addition, biological applicability using mammalian cells and FISH-labeled bacteria will be demonstrated. Moreover, the developed μFACS will be applied to metagenomics (e.g. genomic studies of unculturable baceteria) for purification of bacteria sample and cell-free DNA, which serves as a critical step in obtaining uncontaminated result during genome sequencing.

1.1 Components inside a conventional FACS

While FACS machines have been used widely, the basic components, functionalities, and operation principles have not gone significant changes. The basic components of a benchtop flow cytometer are:

I. A fluidic system to introduce and confine samples to the center of a stream, typically by hydrodynamic focusing

II. An optical system for sample illumination and collection of emitted light

III. A sorting system to deflect cells of interest into respective collection locations

IV. An electronics system for real-time analysis and decision making (if sorting is needed)

Figure 1.1 shows the interior of a simplified version of a four-parameter (two

scattering, forward and side, signals plus two fluorescent signals) flow cytometer. The fluidic system is responsible for the transport of samples through a flow chamber (~ 50-250 μm in diameter). The high-pressure sheath fluid system confines the sample stream to allow cells to pass through optical interrogation region in a sequential manner (e.g. avoid cross-talk between cells). After the cells leave the orifice of the flow cell, the sample stream forms a jet-in-air configuration and become excited by the incoming laser beam (e.g. 488 nm laser). To collect FSC (usually with an angle of bending >5°), a beam stop is required to protect photodetectors from direct illumination (which would result in measuring light extinction, a dip rather than a peak in intensity as a cell passes through the interrogation beam). Side scatter and fluorescence lines are conventionally placed perpendicular to the axis of illumination. Typically FSC and SSC carry implications for the physical characteristics of the cell, as they have some relation to characteristics such as size, refractive index, and internal granularity. Nearly all cytometers further characterize and identify cells by the collection of fluorescence signals emitted from various fluorescent tags. To collect fluorescence signals, the implementation of high-precision, well-aligned, lens-mirror-PMT systems is required. Each PMT detector will register and send the fluorescence signal from a single passband to the electronics for data analysis (namely, differentiating cell samples into different subpopulations). By applying vibrations to the jet flow from the nozzle end, droplets will be formed a fixed distance away from the nozzle after the cells have been interrogated. Cell-containing droplets will then be deflected by electrically charged plates into their respective collection tubes (droplets of no interest flow straight down to

the waste tube without deflection).

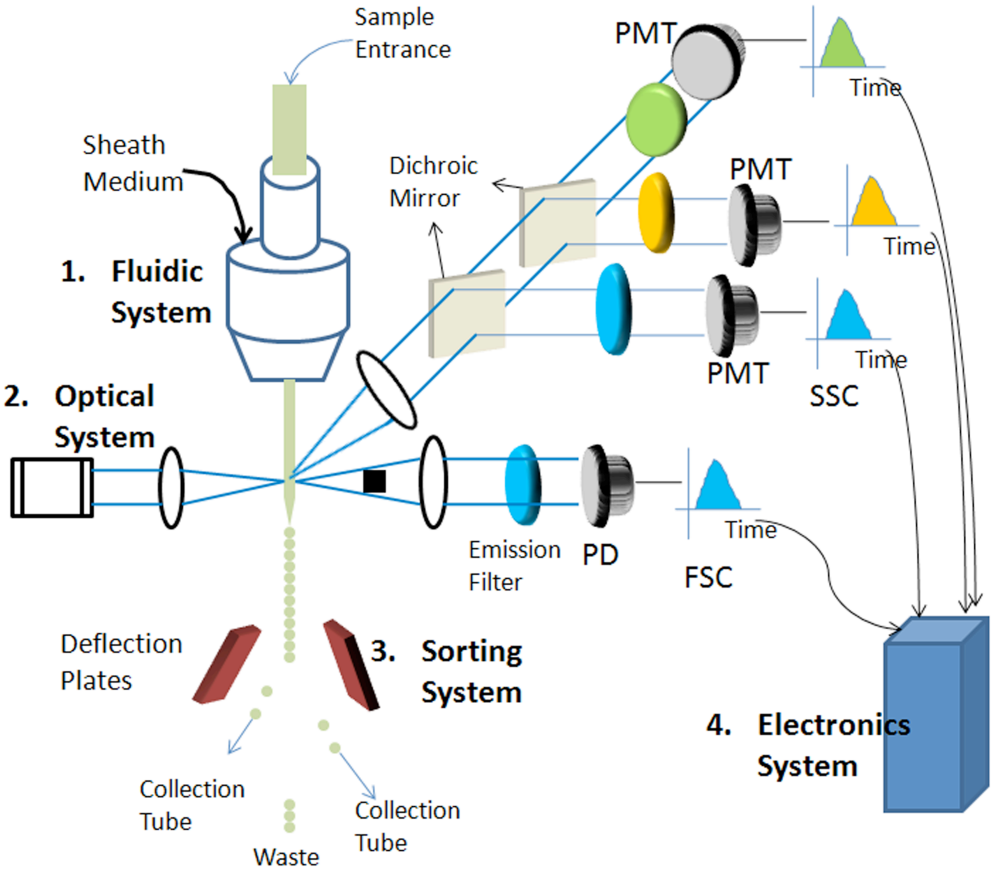

Figure 1.1 Schematic of a 'four-parameter' benchtop flow cytometer

1.2 Single cell analysis and cell sorting

Traditionally researchers study and measure cellular activities in bulk, which result in averaged data information about cell properties. However, even though cells could appear similar morphologically, cellular heterogeneity such as differences in gene expressions, cell proliferations, and responses to external stimuli exists both in bacteria and eukaryotic cells [6-9]. As a result, in order to recover rich information (e.g.

stochastic behavior of individual cells) from cell-based assays, it is essential to analyze cells at the single-cell level.

Single cell analysis has become an important bio-analytical method in basic biological research and the field of diagnostics. For example, in cancer research, tumor cells are highly heterogeneous and single cell analysis enables differentiation of normal and cancer cells and cancer cells at various developmental stages, allowing researchers to peer into tumor initiation, progression, metastasis and therapeutic responses [10]. Similar to cancer cells, stem cells (i.e. embryonic, adult, and induced pluripotent stem cells) are mostly consist of heterogeneous populations [11-13]. By isolating targeted stem cells and analyzing homogeneous populations, researchers have begun to understand their signaling pathways and networks for self-renewal and cell differentiation. Also in diagnostics for instance, preimplantation genetic diagnosis, a prenatal diagnosis that analyzes individual cells extracted from embryos fertilized in vitro, is commonly used to test for genetic diseases and chromosome aneuploidies [14]. Combined with genetic study tools such as PCR and FISH [15], multiplexed PGD using single cell analysis could enable early detection and therefore allowing early treatment of birth defects during embryonic development stages.

Thus, cell sorting (or enrich targeted sub-population from the total population) has become an indispensible tool for most single-cell analysis. Conventionally, cell sorting has been performed using a FACS machine (e.g. FACSAria from BD Biosciences) with sorting capabilities. Because of the significant additional cost incurred by the incorporation of sorting modules, a FACS machine with sorting capability is

typically very costly (> $150k) and bulky (> 400 lb). Lab-on-a-chip FACS offers an alternative platform not only allows significant size and cost reduction but also reduced sample usage and ease of integration of modularized functional units (e.g. upstream sample preparation and downstream cell-culturing). Due to the wide diversity of microfluidic cell sorting technologies, the dissertation only focuses on sorting mechanisms that are compatible with FACS.

1.3 Development of μFACS

As a result of significant advances in microfabrication technologies, numerous microfluidic cell sorters exploiting various sorting mechanisms have emerged. These include sorting based on electroosmosis [16], dielectrophoresis [17], optical gradient forces [18], and hydrodynamic flow switching [19, 20]. Electroosmotic sorters can achieve precise flow switching, but such devices operate under high DC voltage (e.g. hundreds of volts), require frequent change of voltage settings due to ion depletion [21], and suffer from low sorting rate (e.g. tens of particles per sec). On the other hand, DEP-based sorting exhibits precise manipulation down to single cell level, but the throughput is rather limited, as DEP forces eventually become too small relative to the hydrodynamic drag forces with increased flow rates. Although DEP-based sorting can be low-powered and cause minimal cell damage, the fabrication process is fairly extensive and the buffer used requires additional consideration (e.g. ionic conductivity, biocompatibility, etc). An μFACS system using optical forces could be attractive, as thus method could deflect particles or cells in a non-contact manner and operate

independent of fluid flow. However, the use of the bulky high-powered laser as well as the accompanying elaborate optical setup is unfavorable for miniaturization. Additionally, similar to DEP-based sorters, the limitation on flow rates due to the relative weakness of optical forces puts a sever limit on the detection throughput of optical μFACS system. Sorting based on hydrodynamic flow switching, on the other hand, is typically not limited by the imposed flow (or particle) speed, and therefore the method generally offers a high detection throughput (>1,000 cells/s). For instance, Wolff et al. demonstrated fluorescence-activated sorting of 10-μm fluorescent beads from a mixture of beads and chicken red blood cells, achieving a detection throughput of 12,000 cells/s and an enrichment factor of 100-fold [20]. Even though sorting based on hydrodynamic flow switching generally offers high throughput and enrichment capabilities, causes minimal cell damage, and is not subjected to buffer incompatibility issues, the mechanical actuators (e.g. external valves, syringe pumps, and pneumatic pumps) employed usually suffer from limited response times and are generally bulky, thwarting progress toward miniaturization.

To circumvent the use of bulky actuators and further the development toward miniaturization, in this dissertation I will demonstrate two novel sorting mechanisms using an integrated piezoelectric (PZT) actuator to achieve sorting by temporal flow switching. The first sorting module employs the design of an integrated nozzle/diffuser for flow re-direction. Even though the nozzle/diffuser based cell sorting can allow high sorting efficiency (> 90%), the magnitude of the introduced fluid disturbance and the flow flow switching response render the design unsuitable for high-throughput single-

cell sorting. Nonetheless, the method could be useful for on-chip fluid manipulation and flow mixing. To address the aformentioned issues, instead of fluid flow redirection, the integrated piezoelectric (PZT) actuator (response time of 0.1 – 1 ms) achieves sorting by temporal fluid displacement. Besides developing a sorting module, light illumination and collection systems as well as an FPGA-based robust electronics control are developed to enable sorting based on fluorescent emissions from cells. The developed μFACS in this dissertation has a number of merits including

1. High-throughput (> 1,000 cells/s)
2. Fast response time (0.1 – 1 ms)
3. Single-cell manipulation capabilities
4. Low powered sorting actuation (< 10 Vp-p, ~ 1 mW)
5. Sensitivity enhancement through real-time signal amplification
6. Real-time verification of sorting events that allows optimization of sorting parameters in real-time

Table 1 shows a summary of pros and cons of the most commonly used sorting mechanisms. Despite the distinct differences among the sorters, in order for a μFACS system to become useful to biological experiments, the system needs sufficient sorting rate, detection throughput, enrichment factor, and cell viability. I believe the piezoelectric-actuated μFACS in this dissertation not only satisfies all the performance

criteria but also brings about significant size and cost reduction (e.g. inexpensive PZT actuator).

Even though there still exists a gap in term of performances (i.e. sort rates, detection throughput, and purity) between commericial FACS and μFACS, the gap could be bridged by parallel processing and incorporation of a 3-D flow focusing module (reduce velocity variation in z-direction) to increase throughput and purity. In contrast, μFACS in a microfluidic platform possesses several distinct advantages over conventional FACS including reduced sample usage, integration of modular components (e.g. with specific functionalities), disposable, and closed systems. In a conventional flow cytometer, in order to generate ~10^4 of data, a sample of ~ 0.5-1 x 10^6 cells is required [22] whereas in a lab-on-a-chip flow cytometer, analysis of ~10,000-20,000 cells requires a sample of ~ 20,000-30,000 cells. Due to the ease of integration, more functionalities such as sample pre-treatment (e.g. cell lysis) and post-sort cell assays and cell culturing could be readily integrated to the μFACS system enabling a wide range of biological applications (especially in single-cell analysis). Because the μFACS devices are disposable and operate in a closed-system architecture, this avoids the possibility of cross-contamination and exposure to biohazardous agents (e.g. HIV). By exploiting these advantages, I believe the future generations of μFACS systems (likely with more intergrated functionalities) could deeply affect the way biologists perform experiments and may one day replace most bulky FACS machines.

Table 1.1 Comparison between common sorting mechanisms

Sorting Mechanism	Pros	Cons
Electroosmosis	Easy fabrication, simple control, uniform flow pattern	High input voltage (>100 V), ion depletion, low cell viability, low throughput
Dielectrophoresis	Able to trap cells, low-cell damage, flow-independent particle movement	Cell property-dependent, low-throughput, require use of buffer of different ionic strength, complex fabrication
Optical forces	Contactless manipulation, low cell-damage, flow-independent particle movement, high purity	Limited throughput, extensive optical setup (including use of a bulky high-powered laser),
Hydrodynamic	High throughput (>10,000 cells/s), low cell-damage, easy fabrication, high enriching capability	Slow response, require bulky external actuators (e.g. external check valve, syringe pump, and pneumatic pump), low purity
Piezoelectric-actuated	High throughput (>1,000 cells/s), fast response, low cell-damage, easy fabrication, high enriching capability	-

1.4 Thesis Outline

Since μFACS system could provide a number of advantages over conventional FACS, I will focus on the development of a high-throughput piezoelectric-actuated cell sorter and its integration with several novel detection technologies. Eventually the developed technologies will be applied to sort mammalian cells and bacteria for the human microbiome project.

In chapter 2, I will demonstrate a scattering-based detection technology that exploits the signals detected in arrayed waveguides for significant signal amplification. The insights gained from this study will be applied to fluorescence detection in chapter 5.

In chapter 3, I will demonstrate the first generation of the sorting module using principle of 'Nozzle-Diffuser'. Even though the sorting module is unsuitable for high-throughput operation, the fluid displacement ability we observed from the operation leads me to design the second generation sorting module which will be discussed in chapter 4.

In chapter 4, I will demonstrate the design, fabrication, and characterization of a low-powered fast-response piezoelectric-actuated cell sorting module. Dynamic simulation and characterization of frequency-response and deflection magnitude response will be shown. From the characterization, it is determined that the sorting module could support high-throughput operation at low power and cost.

In chapter 5, integration of fluorescence detection technology and piezoelectric sorting module into a μFACS technology will be shown. Because of the novel design of the detection technology, sorting parameters can be optimized in real-time. This capability is unseen in other μFACS technologies. Sorting efficiency will be characterized. The integrated μFACS will also be used to enrich samples including beads and mammalian cells. We will show the enrichment is the highest among μFACS systems and the performance is comparable to commercial FACS.

In chapter 6, the integrated μFACS will be applied to metagenomics. Using the integrated μFACS, we will address two specific challenges in metagenomics, detection sensitivity and cell-free DNA contamination. Sensitivity improvements in sample fluorescent labeling and light focusing using two-step optofluidic waveguide will be discussed. Moreover, cell-free DNA removal capability of the μFACS will be characterized and compared to commercial FACS. In addition, proof-of-concept sorting of rare bacteria will be done to show the feasibility in isolation of uncultivated bacteria.

References:

[1] A. Moldavan, "Photo-electric technique for the counting of microscopical cells," Science, vol. 88, pp. 188, 1934

[2] E. O. Casamayor, I. Ferrera, X. Cristina, C. M. Borrego, and J. M. Gasol, "Flow cytometric identification and enumeration of photosynthetic sulfur bacteria and potential for ecophysiological studies at the single-cell level," Environmental Microbiology, vol. 9, pp. 1969-1985, 2007.

[3] J. W. Gratama, Alberto Orfao, David Barnett et al. "Flow Cytometric Enumeration of CD34+ Hematopoietic Stem and Progenitor Cells," Cytometry, vol. 34, pp. 128-142, 1998.

[4] L. A., Herzengberg, D. Parks, B. Sahaf , O. Perez , M. Roederer, "The history and future of the fluorescence activated cell sorter and flow cytometry: a view from Stanford," Clin. Chem., vol. 48, pp. 1819-1827, 2002.

[5] J. Godin, C.-H. Chen, S. H. Cho, W. Qiao, F. Tsai, and Y.-H. Lo, “Microfluidics and photonics for Bio-system-on-chip: A review of advancements in technology towards a microfluidic flow cytometry chip,” J. Biophoton, vol. 3, pp. 1-22, 2008.

[6] J. S. Marcus, W. F. Anderson, and S. R. Quake, “Parallel picoliter RT-PCR assays using microfluidics,” Anal. Chem., vol. 78, pp. 956–958, 2006.

[7] J. E. Ferrell and E. M. Machleder, “The biochemical basis of an all-or-none cell fate switch in xenopus oocytes,” Science, vol. 280, pp. 895–898, 1998.

[8] T. Y. Huang, T. F. Chu, H. I. Chen, and C. Y. Jen, "Heterogeneity of [Ca2C]i signaling in intact rat aortic endothelium," FASEB J., vol. 14, pp. 797–804, 2000.

[9] M. N. Teruel and T. Meyer, "Parallel single-cell monitoring of receptor-triggered membrane translocation of a calcium-sensing protein module," Science, vol. 295, pp. 1910–1912, 2002.

[10] Y. He, J. Wu, D. C. Dressman et al. (2010). "Heteroplasmic mitochondrial DNA mutations in normal and tumour cells," Nature, vol. 464, pp.610-614, 2010

[11] T. Graf and M. Stadtfeld, "Heterogeneity of embryonic and adult stem cells," Cell Stem Cell, vol. 3, pp. 480-483, 2008.

[12] K. Takahashi, K. Tanabe, M. Ohnuki et al. "Induction of pluripotent stem cells from adult human fibroblasts by defined factors," Cell, vol. 131, pp. 861–872, 2007.

[13] J. A. Shizuru, R. S. Negrin, and I. L. Weissman, "HEMATOPOIETIC STEM AND PROGENITOR CELLS: Clinical and Preclinical Regeneration of the Hematolymphoid System," Annual Review of Medicine, vol. 56, pp. 509-538, 2005.

[14] K. Sermon, A. V. Steirteghem, and I. Liebaers, "Preimplantation genetic diagnosis," Lancet, vol. 363, pp. 1633-41, 2004.

[15] S. Munne, J. Grifo, J. Cohen, and H. U. Weier, "Chromosome abnormalities in human arrested preimplantation embryos: a multiple-probe FISH study," Am. J. Hum. Genet., vol. 55, pp. 150–159, 1994.

[16] A. Y. Fu, C. Spence, A. Scherer, F. H. Arnold, and S. R. Quake, "A microfabricated fluorescence-activated cell sorter," Nat. Biotechnol., vol. 17, pp 1109-1111, 1999.

[17] D. Holmes, M. E. Sandison, N. G. Green, and H. Morgan, "On-chip high-speed sorting of micron- sized particles for high-throughput analysis," IEEE Proceedings-Nanobiotechnology, vol. 152, pp. 129–135, 2005.

[18] M. M. Wang, E. Tu, E. R. Daniel, et al. "Microfluidic sorting of mammalian cells by optical force switching," Nat. Biotechnol., vol. 23, pp. 83-87, 2005.

[19] J. Krüger, K. Singh, A. O'Neill, C. Jackson, A. Morrison, and P. O'Brien, "Development of a microfluidic device for fluorescence activated cell sorting," Journal of Micromechanics and Microengineering, vol. 12, pp. 486–494, 2002.

[20] A. Wolff, I. R. Perch-Nielsen, U. D. Larsen, et al. "Integrating advanced

functionality in a microfabricated high-throughput fluorescent-activated cell sorter," Lab Chip, vol. 3, pp. 22–27, 2003.

[21] A. Y. Fu, Microfabricated Fluorescence-Activated Cell Sorters (FACS) for Screening Bacterial Cells, thesis Ph. D. Pasadena: California Institute of Technology

[22] C. E. Sims, and N. L. Allbritton, "Analysis of single mammalian cells on-chip," Lab Chip, vol. 7, pp. 423-440, 2007.

Chapter 1 or portion thereof has been published in ***Tay & Francis Group*****,**

Handbook of Optofluidics, ch. 19 (2010)

Chapter 2

Advanced detection technology for microfluidic flow cytometer

In a conventional FACS machine, detection of biological agents is achieved using one light source (e.g. 488 nm laser) and multiple light detectors (e.g. PMTs) to register scattering and fluorescent signals. In this detection scheme, each detector samples one scattering/fluorescent signal for each laser excitation. The scheme does not allow signal enhancement from post signal processing (Figure 2.1 (A)). In contrast, since microfabrication guarantees pre-aligned device architecture, it is fairly

straightforward to design a device structure that enables oversampling of emission signals from individual analytes as shown in figure 2.1 (B). The advantage of processing multiple emission signals from one analyte is that once the relationship between these signals can be deciphered, we can exploit this feature to amplify detected signals. This chapter describes an arrayed waveguide structure, which is designed to allow amplification of signals resulting from multiplexing of signals. In addition, detection method used in chapter 4 also exploits the feature of oversampling for sensitivity enhancement in a slightly different way (off-chip light collection). Amplification is essential in biological detection especially when encountering weak emission signals (e.g. surface-marker labeled cells or FISH-labeled bacteria).

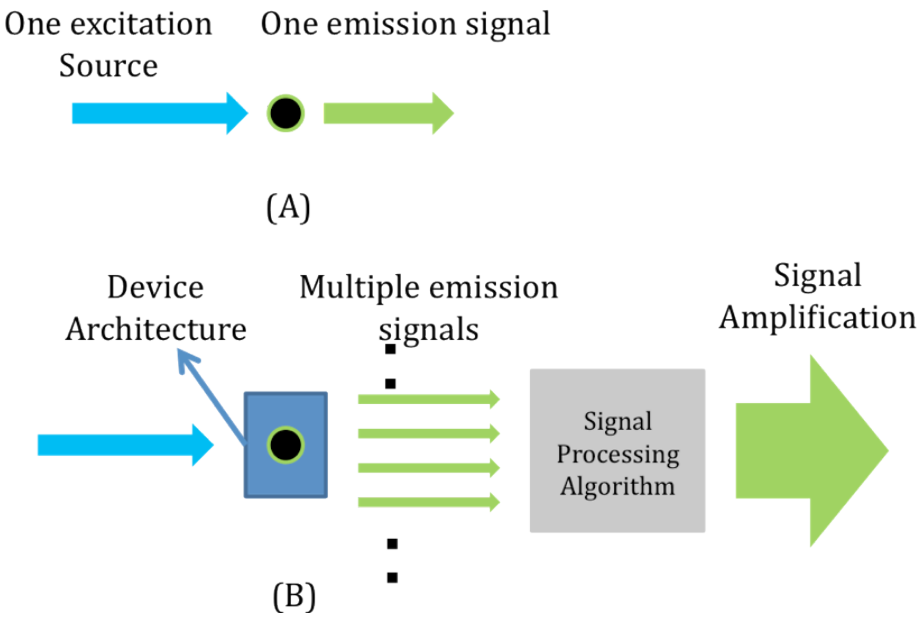

Figure 2.1 Detection methodology. (A) Conventional detection employs one excitation one collection system. (B) Oversampling of multiple emissions enables signal amplification using a signal processing algorithm.

2.1 Integrated arrayed waveguides for scattering detection

Lab-on-a-chip flow cytometry has been a fast-growing field and significant progress has been made in improving its functionality and sensitivity. Sensitivity enhancement has been highly facilitated by the significant progress in on-chip waveguide-fabrication technology. Light coupling through planar arrayed waveguide has been demonstrated to detect fluorescent particles with high sensitivity using the cross-correlation amplification algorithm [1]. However, particles traveling at speeds different from their estimated velocities in the microfluidic channel were simply left undetected. In this chapter, we will demonstrate highly sensitive scattering-based detection on the planar platform containing a pair of symmetric optical arrayed waveguides. The fabrication of the device, which consists of fluidic channels and arrayed waveguides, is inexpensive (re- quires only two types of polydimethylsiloxane (PDMS) of different refractive indices) and relatively simple. The integrated photonic-fluidic device enables implementation of on-chip arrayed-waveguide excitation and detection with only a simple light source and a detector. Combining the device architecture with the proposed signal processing algorithm, sensitivity enhancement (80 dB enhancement relative to the untreated signals) and accurate velocity measurement of particles/cells can be achieved. Moreover, the validity of the processed signals is further verified under a conventional charged-coupled-device (CCD) microscope detection scheme showing excellent correspondence.

2.2 Symmetric arrayed-waveguide fabrication and operation

The device fabrication employs conventional microreplica-molding technique [2] and monolithic integration of optical waveguides using the capillary filling method [1]. The device substrate (e.g., cladding layer) is made of PDMS with refractive index of 1.407. The core material (Gelest OE 42, Gelest Inc.) with a refractive index of 1.42 is introduced into the arrayed waveguide channels for 1 h by capillary filling. The device is cured in the 90 °C oven for 8 h prior to use.

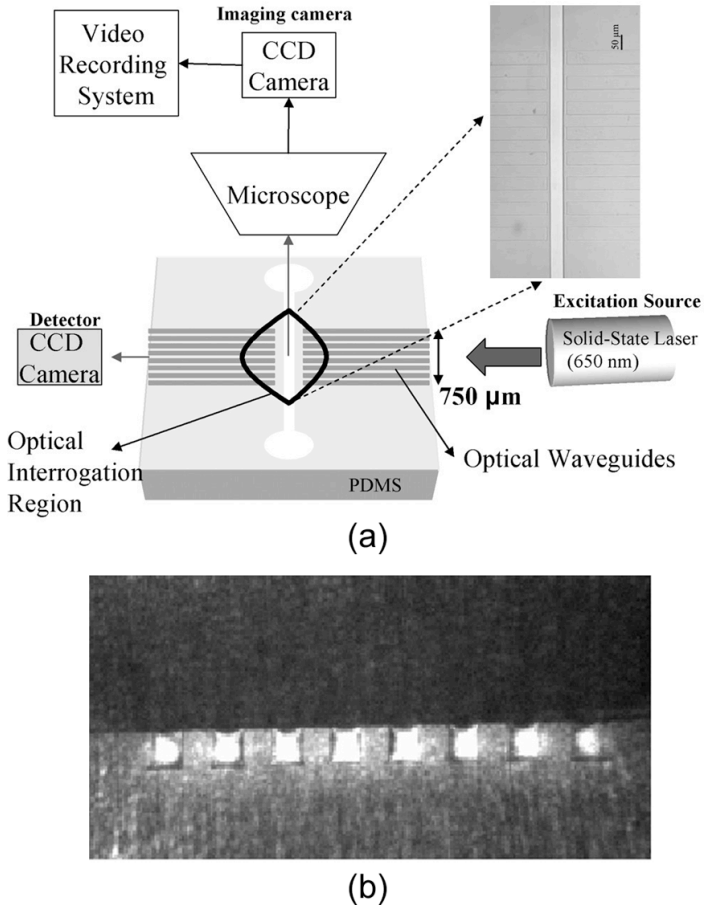

Figure 2.2 (a) Scattering-based experimental schematics. Eight planar waveguides couple excitation light into the fluidic channel while the other eight waveguides couple the light to the detector. Multimode, buried heterostructure waveguides are formed with PDMS core (n = 1:42) and cladding (n = 1:407). (b) Image of the output waveguide array. The laser light emanating from each waveguide is collected and monitored by the CCD camera. Light intensity is recorded and further used for signal amplification.

The experimental setup of the scattering-based detection scheme and the symmetrical arrayed-waveguide structure is depicted in Fig. 2.2(a). With a simple excitation light source (semiconductor diode laser, nm), the device architecture allows

highly localized excitation and detection in the optical IR. One set of input waveguides couple excitation light to the IR while the output waveguides couple the light to the detector. The transmitted light at the end of the output waveguides is shown in Fig. 2.2(b) and light intensity integrated over the individual waveguide cross section area is detected and recorded by the CCD detector. As particles pass by the IR, incoming light from the excitation waveguides will be scattered (e.g. extinction) resulting in successive lowering of light intensity detected from one waveguide to the other. Since every particle travels at a specific speed (i.e., assuming particles experience negligible acceleration within the optical IR), the signals from each waveguide are correlated in time domain. Due to this property, the integrated device architecture offers a simple, yet highly sensitive detection scheme that provides the basis for time-delay-based signal amplification.

2.3 Signal processing algorithm

The arrayed-waveguide structure enables sensitivity enhancement by over-sampling (e.g., signals from eight waveguides) based on the fact that signals detected from each waveguide are correlated in time domain. Block diagram of the amplification algorithm is depicted in Figure 2.3. First, high-pass filters (HPFs) are used to remove low-frequency noise (i.e., reduces the likelihood of amplifying false signals) caused by the semiconductor laser. The effect of passing through the HPF is seen by comparing Figure 2.3(a) and 2.3(b), where laser-induced intensity fluctuations have been removed. Next, by assuming discrete time delays (i.e., time interval for one particle to travel from one waveguide to the next), signal amplification is carried out by the following

algorithm:

$$S_n(t) = S_1(t) \bullet S_1(t+\Delta_n) \bullet S_1(t+2\Delta_n) \bullet \ldots \bullet S_8(t+7\Delta_n) \quad (1)$$

where n is the number of frames taken by the detector (i.e., if n=2 and the frame rate is 52.6 frames per second, Δ_2 =time elapse of two frames or 0.038 s) and $S_n(t)$ is the amplified signal for each assigned time delay. Conceptually, amplification occurs only when the particle velocity matches the assumed time delay (top of figure 2.3). Fig. 2.4(c) shows an example of an amplified signal by assuming Δ_2= 0.038 s. In this case, signals that are correlated with the specified time-delay will be amplified (shown by the distinct peaks in figure 2.4(c)). As can be seen in the figure, before applying the signal amplification algorithm, most signals are indistinguishable from noise (Fig. 2.4(a)), which is caused by the shot noise, CCD camera's thermal noise, and the intensity fluctuation of the semiconductor laser diode. However, after implementing the signal processing algorithm, the amplified signals (Figure 3(c)) from a sample of 5-μm beads allow clear identification of particles. Every pronounced peak represents one 5-μm particle passing through the IR at a given time. In addition to sensitivity enhancement, the employed algorithm permits accurate velocity measurement. Velocity measurement is based on the knowledge of the assigned time delays, and distance between adjacent waveguides ($V_n = D_w/\Delta_n$, where D_w is the distance between adjacent waveguides). V_n is

the estimated velocity for the given Δ_n. In this algorithm, velocity estimation is done prior to the amplification algorithm [equation (1)] and is quantized due to the frame rate of the detector. Beads that travel at the predetermined velocity will be amplified while beads traveling at other speeds will not be amplified. In Figure 3(c), the velocity estimation is carried out by assuming $\Delta_2 = 0.038$ s (i.e., two frames) and as a result, only the beads that are traveling at 2.63 mm/s are detected (shown as amplified peaks). In a similar fashion, particles traveling at other speeds can also be detected by assuming different time delays. The last step of the algorithm is the summation of all the amplified signals, each of which assumes incremental time delay, which is limited by the frame rate of the detector.

The summed signals, $S_T(t)$ from a sample of 5- m beads traveling at different velocities are shown in Fig. 3(d). Due to the laminar and fully developed flow condition (Reynolds number $Re < 1$) [3], the velocities of the particles in the microfluidic channel would vary spatially (i.e., across the channel). Nonetheless, the proposed algorithm is capable of detecting particles of different velocities and can be easily extended to detect particles in real time.

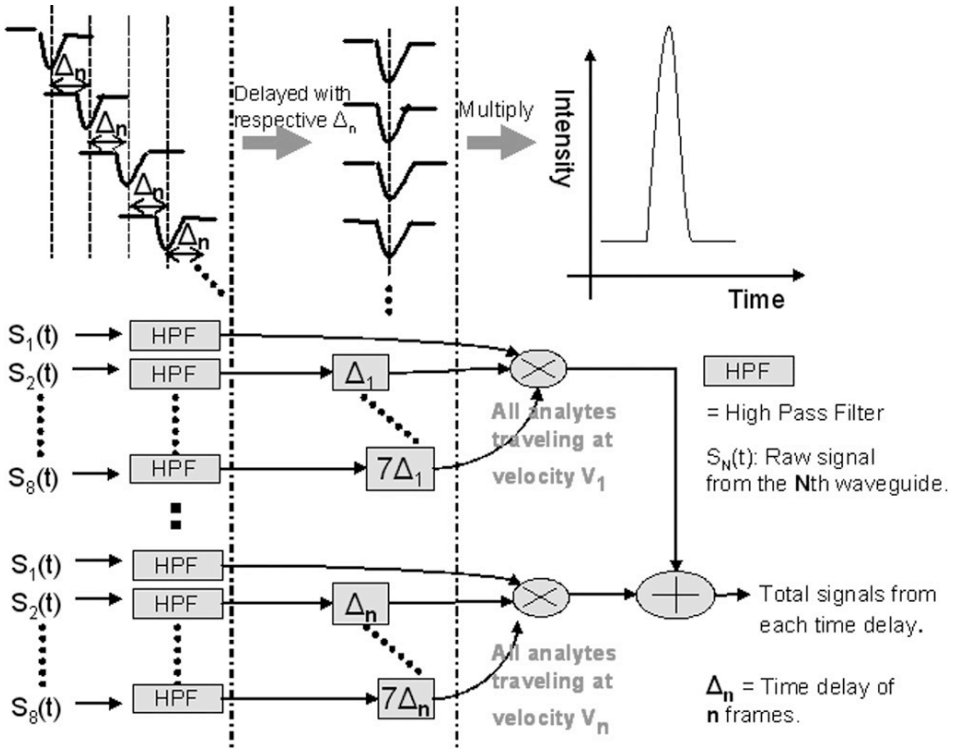

Figure 2.3 Block diagram for the multiplication-based cross correlation algorithm

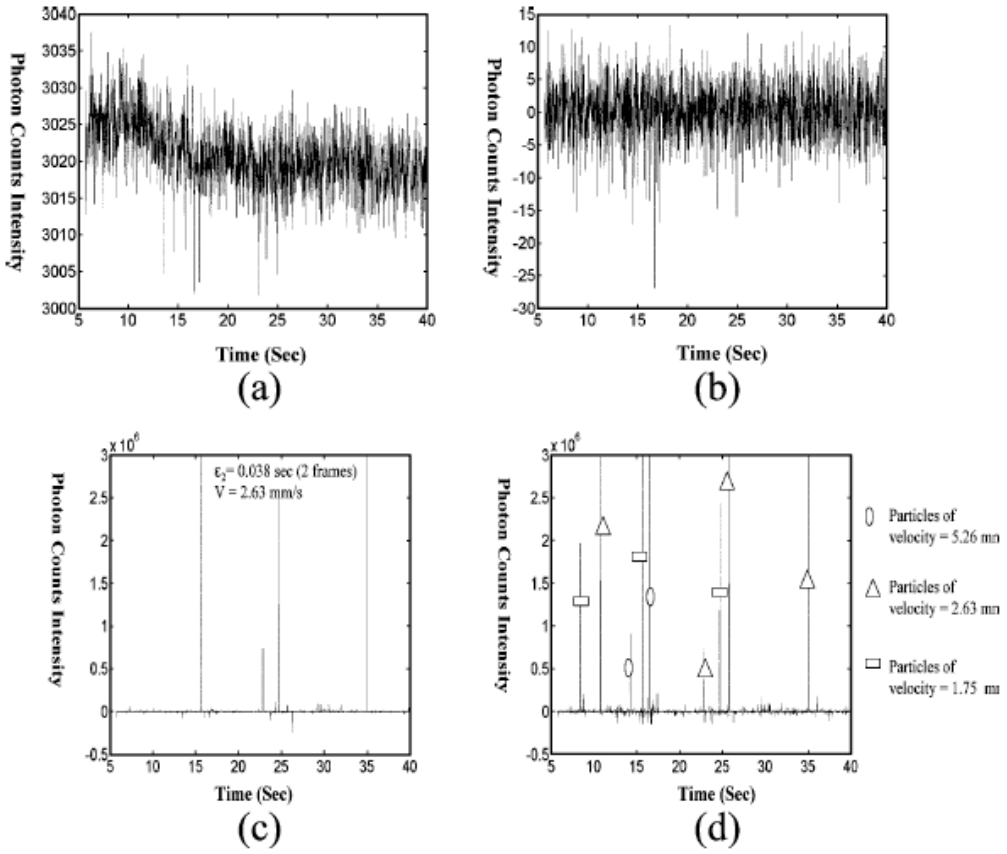

Figure 2.4 Signals from a sample of 5-_m beads. Raw signal from one of the eight waveguides is shown in (a). After passing through the HPF, (b) the low-frequency noise is removed. By assuming a specific time delay (e.g., 0.038 s in this case), multiplication-based signal amplification is carried out and shown in (c), and at the same time, velocity measurement is done based on the assigned time delay. Each peak represents one 5-_m bead traveling through the IR with velocity of 2.63 mm/s. (d) Summation of the amplified signals from each incremental time delay (or velocity) and beads of different velocities are labeled with different geometric figures.

2.4 Signal verification and analysis

To verify the amplified signals, another CCD camera is connected to the microscope to display the top view of the device in real time. Analysis of frame-by-frame images from the recorded video has shown that eight particles of different velocities have been identified. The amplified signals have captured nine particles within the given time period, including all eight particles identified by the video and the extra bead that was hard to observe from the video image due to motion-induced blurring. In addition, the measured speed of each bead agrees well with the speed extracted from the video imaging, which validates the device architecture and the algorithm. The fact that the amplified result has shown highly enhanced signals and captured one additional particle not initially observed in the video [the first peak in Fig. 2.4(d)) demonstrates the superior sensitivity of the method over the conventional microscope-CCD detection scheme, in addition to tremendous cost and size reduction. The estimated enhanced signal-to noise ratio (SNR) relative to the raw signals is 80 dB. As opposed to cross multiplication, another conventional signal processing algorithm employs summation of signals with respective time delay. The multiplication method shows significant SNR improvement over summation method with dB in the range from 20 to 70 in our case. However, the estimated minimum number of waveguides needed for the proposed design architecture and the algorithm is five pairs of symmetrical waveguides. Any value below this number would cause the algorithm to produce noise that becomes comparable to the amplified signals.

2.5 Conclusion

We have demonstrated a simple, yet highly sensitive, arrayed-waveguide excitation and detection scheme based on scattering effect. The signal processing algorithm allows sensitivity enhancement and velocity measurement. Processed signals are confirmed by the video recording showing accurate correspondence. The developed platform can easily be applied to count suspended microbeads and cells in the fluid and measure their velocities with high sensitivity in real time.

In addition, the signal algorithm developed here provides several key insights (signal modulation could give rise to signal amplification) in the development of the fluorescence detection technology, which will be discussed in chapter 5.

References:

[1] V. Lien, K. Zhao, Y. Berdichevsky, and Y.-H. Lo, "High-sensitivity cytometric detection using fluidic-photonic integrated circuits with array waveguides," IEEE J. Sel. Topics Quantum Electron., vol. 11, no. 4, pp. 827–834, 2005.

[2] Y. Xia and G. M. Whitesides, "Soft lithography," Annu. Rev. Mater. Sci., vol. 28, pp. 153–184, 1998.

[3] P. K. Kundu and I. M. Cohen, *Fluid Mechanics*. San Diego: Elsevier Academic Press.

Chapter 2 or portion thereof has been published in ***IEEE Photonics Technology Letter,*** **vol. 19, Iss. 6, pp. 441~443 (2007).**

Chapter 3

Nozzle-Diffuser driven cell sorting module

Even though Nozzle/diffuser pumps have been a well studied field [1-4], most of the studied have been concentrated on characterization and optimization of flow behavior (e.g. pumping rates and rectification efficiencies) both numerically and experimentally under different operating conditions (i.e. actuation frequency and amplitude) and design architectures such as diffuser length, angle, and shape. In one study, Gerlach has shown that the pumping effect would become reversed at large diffuser angle (e.g. 70˚) and that the optimal rectification efficiency occurs at the angle

of ~ 5˚. Besides design optimization, different flow-generating pumping methodologies including thermopneumatic [5], electromagnetic [6], and piezo-to-lever actuations [7] have been implemented to allow increased membrane deflection and pumping rate as well as off-chip actuation control. However, the applications of these pumps have only been shown to transporting of different fluids and cells across the microchannels [8, 9]. The potential of flow switching based on nozzle-diffuser principle has yet been investigated. Also, most of the nozzle/diffuser devices (made of silicon or plastics) are conventionally fabricated using labor-intensive micromachining and silicon-etching methods, which render cost per device high. In contrast, device fabrication (made of polydimethylsiloxane (PDMS)) using the conventional micro-replica method can significantly reduce the cost and therefore, make the device truly disposable.

In this chapter, we will integrate a highly efficient nozzle/diffuser-based particle sorting module onto a PDMS substrate, using a unimorphic piezoelectric (PZT) membrane as the actuator. The device fabrication process is greatly simplified by the technique of adhesive-free, UV Ozone bonding. This novel copper-PDMS bonding technique also allows optimal energy transmission from the PZT actuator to the fluid. The device is shown to be able to manipulate bubble trajectory and sort beads with high efficiency based on the principle of hydrodynamic flow-switching.

3.1 Principle of Nozzle-Diffuser

Nozzle-Diffuser pump is a valveless pump which achieves a biased net flow toward the designed direction by exploiting the differences in pressure loss across the

nozzle and diffuser structure. Figure 3.1A demonstrates the basic operation principle of a nozzle-diffuser. Figure 3.1B shows that the flow resistance for a nozzle is higher than for a diffuser. As the membrane draws/pushes fluid in/out periodically, due to the differences in fluid resistance (pressure loss), net flow (e.g. time-averaged flow) is driven to the right.

To design a nozzle-diffuser structure that optimizes the net flow, it is important to consider the pressure head loss due to the viscous effect of fluid,

$$\Delta P_{loss} = (1/2)*V^2*\xi \qquad (1)$$

where V is the mean flow velocity and ξ is pressure loss coefficient. V is controlled by the frequency and magnitude of the membrane deflection and ξ is dependent upon channel geometry (such as θ and L in figure 3.1B) as well as the roundness of the diffuser/nozzle neck (e.g. the entrance of a nozzle/diffuser).

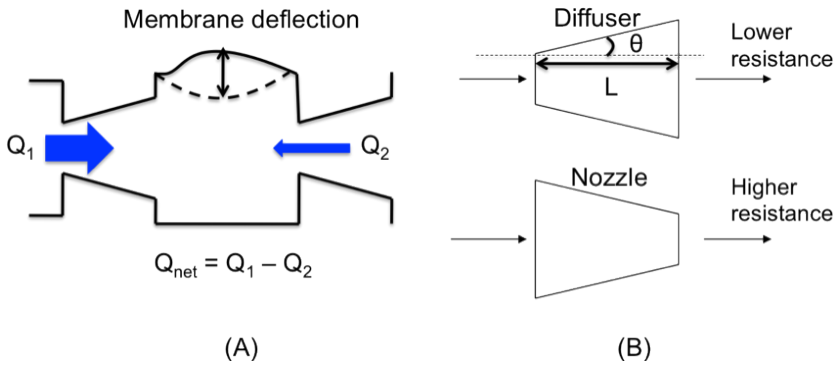

Figure 3.1 Principle of a nozzle-diffuser pump. (A) Net flow toward the right is created by membrane deflection. (B) Fluid resistance is higher for a nozzle structure than for a diffuser structure.

3.2 Characterization of nozzle-diffuser pumps

In order to integrate a nozzle-diffuser structure to perform cell sorting, it is essential to characterize various proposed nozzle-diffuser structure designs and determine ones that have sufficient rectification efficiency (ability to create biased net flow). Several nozzle-diffuser architectures have been designed including a few that employ cascaded structures (more than one diffuser/nozzle in one direction). Membrane structure is created by bonding a piezoelectric disk, which will be discussed in subsequent sections, to the microfluidic device. Net flow (e.g. flowrates) for each structure is characterized as a function of frequency shown in figure 3.2. As expected, at relative low frequency operation, flowrates are proportional to the applied frequency. However, different structures yield different flowrates for a given frequency. We believe to integrate the optimized sorting module, the nozzle-diffuser structure should give optimized rectification efficiency (highest flow rates). Thus, the cascaded structure with vertical offset is implemented to achieve sorting by flow re-direction.

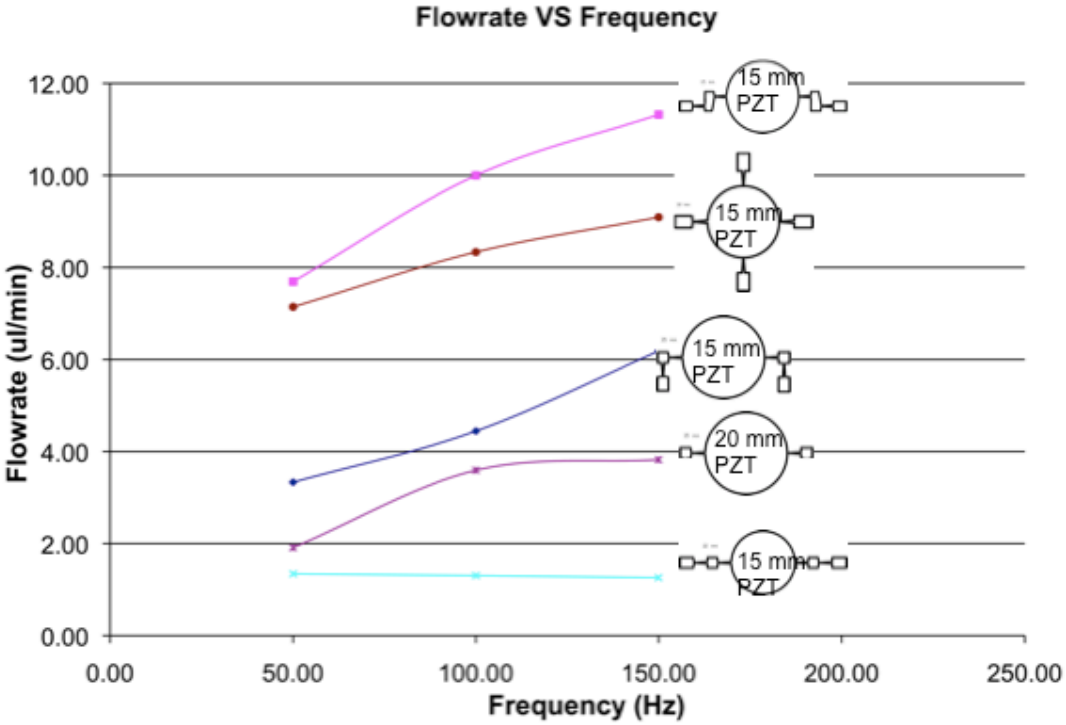

Figure 3.2 Characterization of designed nozzle-diffuser pumps.

3.3 Design and theory of the cascaded nozzle-diffuser cell sorter

In the sorter design, the nozzle/diffuser pump is employed as the driving force for fluid manipulation and particle sorting. Two essential device features, cascaded nozzle/diffuser structure with vertical offset and rounded edges in the neck region of the diffuser, are incorporated into the device structure. Compared to conventional 1-to-1 diffuser inlet and outlet under PDMS substrate, our experiment shows that the cascaded structure has a 30% enhancement of pumping flow rate. Figure 3.3B shows the essential design parameters of the nozzle/diffuser. The diffuser length is 2.5 mm long with a diverging angle of $\theta \approx 5^{\circ}$ and the rounded edge of the diffuser neck has a radius of 50

μm. The parameters used here are the optimized values according to previous studie [3]. In addition, the main fluid channel has a dimension of 50 x 50 um and the actuation chamber has a diameter of 12.5 mm and a depth of 1 mm. Sorting is accomplished having the particle-carrying fluid entering the fluid inlet, traveling down to the intersection area, and reaching the outlet of the nozzle/diffuser. Without PZT actuation, the particle travels directly down and exits through the outlet of the main fluidic channel; whereas when PZT actuator is turned on, the fluid gets directed to the right making a 90˚ turn into the actuation chamber (figure 3.3A).

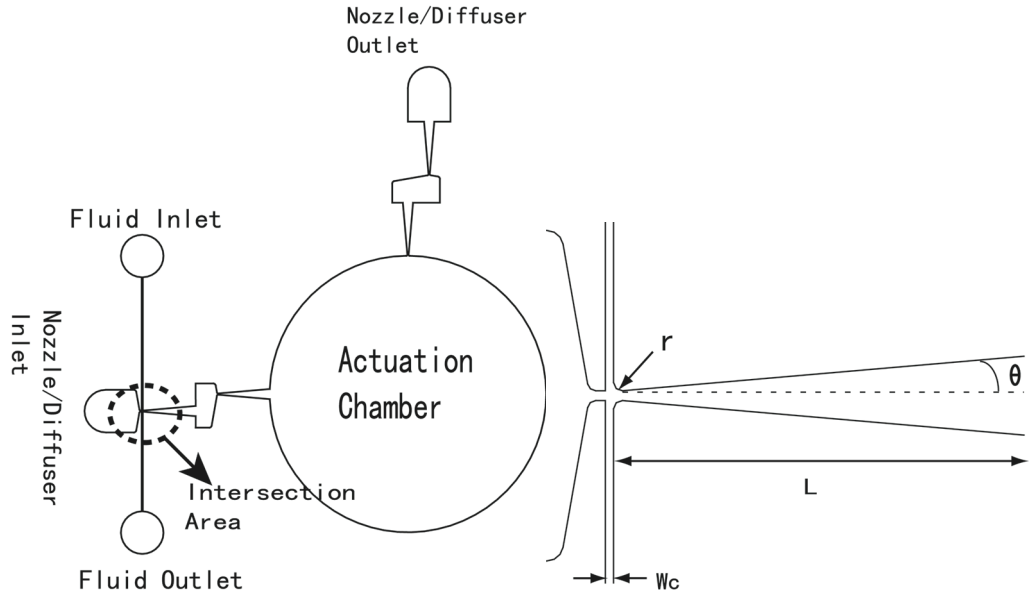

(A) (B)

Figure 3.3 (A) Device architecture that consists of two cascaded nozzle/diffuser structures with vertical offsets. (B) Enlarged view of intersection area showing critical design parameters.

3.3.1 Cascaded nozzle-diffuser simulation

Even though transient effects of the nozzle/diffuser sorting capability is not simulated due to the complexity of the problem, static steady-state simulations for on-off actuation modes have been done using Comsol 3.3 (Figure 3.4). With water as the fluid, the simulation assumes incompressible flow; and therefore, incompressible continuity and Navier-Stokes equations are used to solve for resulting flow pattern.

$$\nabla \cdot \mathbf{v} = 0 \tag{2}$$

$$\rho((\partial \mathbf{v}/\partial t) + \mathbf{v} \cdot \nabla \mathbf{v}) = -\nabla P + \mu(\nabla^2 \mathbf{v}) + \rho \mathbf{g} \tag{3}$$

ρ is the fluid density (~1000 kg/m^3 for water), **v** is the velocity field, P is the pressure, μ is the dynamic fluid viscosity (~1.002 × 10^{-3} N s/m^2 for water), and **g** is the gravity constant. Generally, microfluidic flow conditions are laminar and gravity is negligible and as a result, nonlinear and gravity terms drop out of equation (2). During off actuation state (i.e. PZT actuator is turned off), to ensure the sample flow entering the fluid inlet (with V_{avg} ~ 20 mm/s) would travel straight down and exit through the outlet of the fluidic channel as opposed to exiting toward diffuser inlet and outlet, constant hydrostatic pressure of approximately 1 kPa is imposed on both diffuser inlet and outlet. As the described boundary conditions are imposed, flow converges in the intersection region and exits from the outlet of the main channel. When the PZT actuator is turned

on with a sinusoidal voltage signal, a constant pressure gradient between the nozzle/diffuser inlet and the outlet is produced, in addition to the pre-imposed hydrostatic pressure. The pressure gradient created is equal to the back pressure of the nozzle/diffuser pump, which has a value of ~ 500 Pa in this design. Also, a periodic nozzle/diffuser flow is present at the frequency of the applied voltage signal. However, for a viscous flow in microfluidic channel, this effect is often negligible (i.e. the fluid appears to be pumped continuously toward the diffuser outlet) when the frequency of applied voltage is higher than the frequency response of the system. This justifies the use of simplified steady-state simulation for characterization of the flow behavior.

With the introduction of the pressure gradient between the nozzle/diffuser inlet and outlet, steady-state simulation shows the redirection of flow pattern into the diffuser region (Fig. 3.4). Streamline plots show that the fluid entering fluid inlet (i.e. fluid from top) is directed to the diffuser region (i.e. to the right) as PZT actuator is turned on as opposed to moving straight down when PZT actuator is turned off.

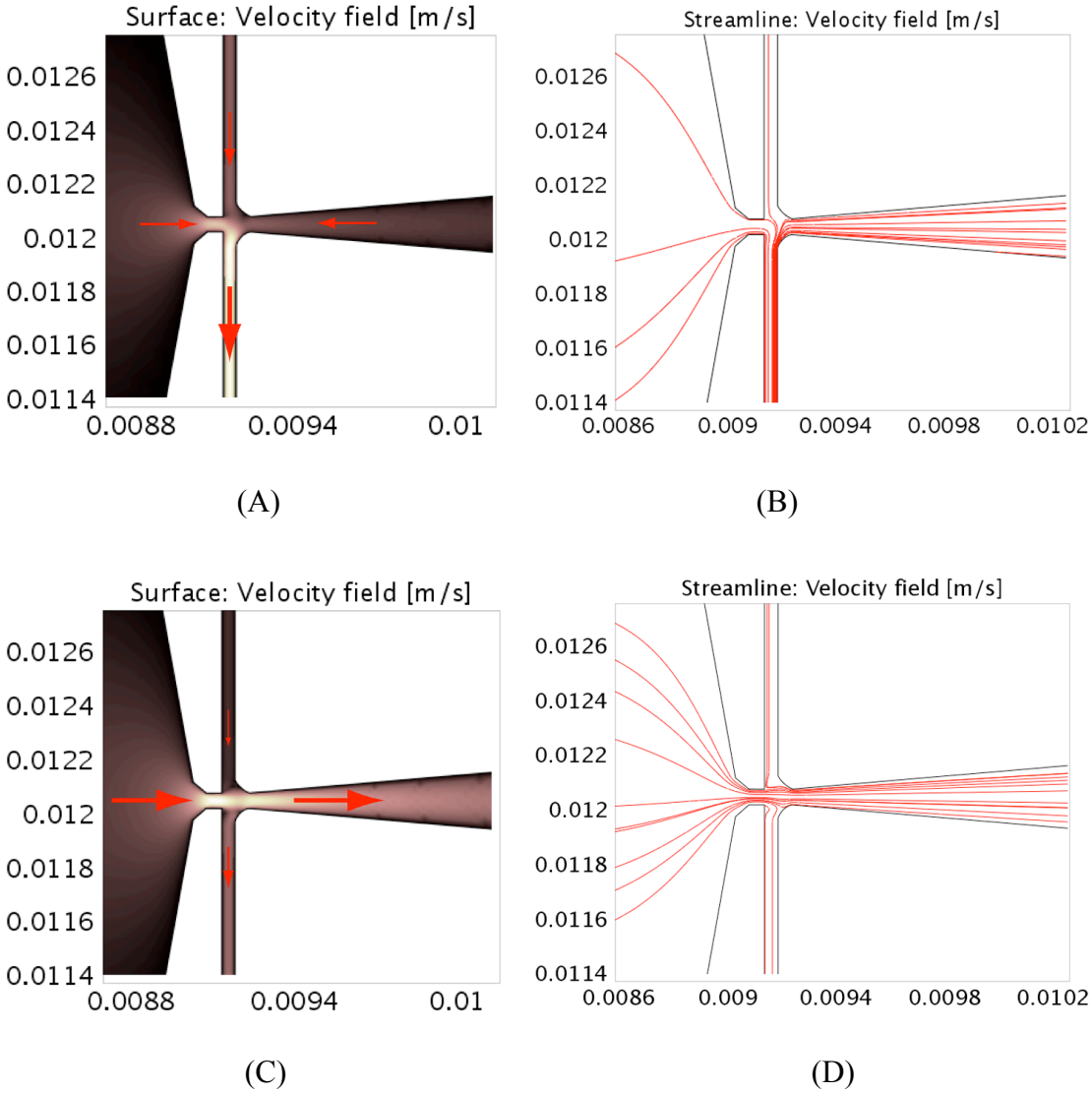

Figure 3.4 Magnitude of simulated velocity field is shown in a) and c), and the respective stream plots are shown in b) and d). Flow pattern in off state of PZT actuator is shown in a) and b), showing converging flow at the intersection region. During on state of PZT actuator, c) and d) show, instead of a converging flow, fluid entering from the top is being drawn to the right and eventually to the nozzle/diffuser outlet.

3.3.2 Device Fabrication

The device fabrication uses conventional microreplicamolding technique [10] in which device features are photolithographically defined by SU-8 photoresist mold using a chrome mask. For device assembly, we have developed a simple yet effective bonding methodology using UV Ozone. Exposure to UV Ozone activates glass, PDMS, and PZT (e.g. copper) surfaces for bonding. After PDMS demolding and punching a 12.5 mm diameter hole through PDMS to form the actuation chamber, the PDMS substrate (Sylgard 184, Dow Corning) is sealed off with a glass slide by UV Ozone bonding (i.e. 3-minute UV ozone treatment of glass and PDMS surfaces) in a UV ozone cleaner chamber (Jelight Inc., Irvine) with a lamp output of 28 mW at 254 nm. For the subsequent PZT actuator and PDMS substrate bonding, the copper surface of the PZT actuator is first UV Ozone treated for 10 minutes, followed by treating both PDMS substrate and copper surfaces for another 5 minutes (Figure 3.5A). To enhance bonding strength, the assembled device is then transferred to an 85 ˚C oven for 8 hours. Fig. 3.5B shows the overall structure of the device. The strong copper-to-PDMS bonding (i.e. bonding strength of ~ 30 kPa) has the advantages of preventing fluid leakage and optimization of power transmission due to direct physical contact between PZT actuator and liquid.

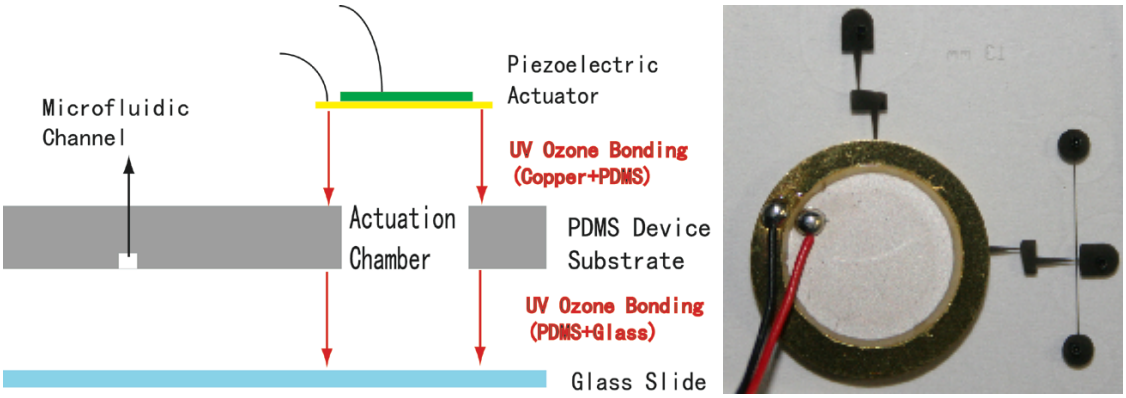

(A) (B)

Figure 3.5 A) Device fabrication using two-step UV Ozone bonding processes. This process enables tight seal between PZT actuator and PDMS. B) The image of the nozzle/diffuser sorter device.

3.4 Experimental results

3.4.1 Bubble sorting experiment

To impose desired hydrodynamic pressure to the nozzle/diffuser inlet and outlet (e.g. to achieve converging flow toward fluid outlet when PZT actuator is in off state), water columns with adjustable vertical height are used. Syringe pump (NE1000 era pump) is used to establish constant flow rate (i.e. constant average speed of particles) and the PZT actuator is driven by an AC voltage source (figure 3.6).

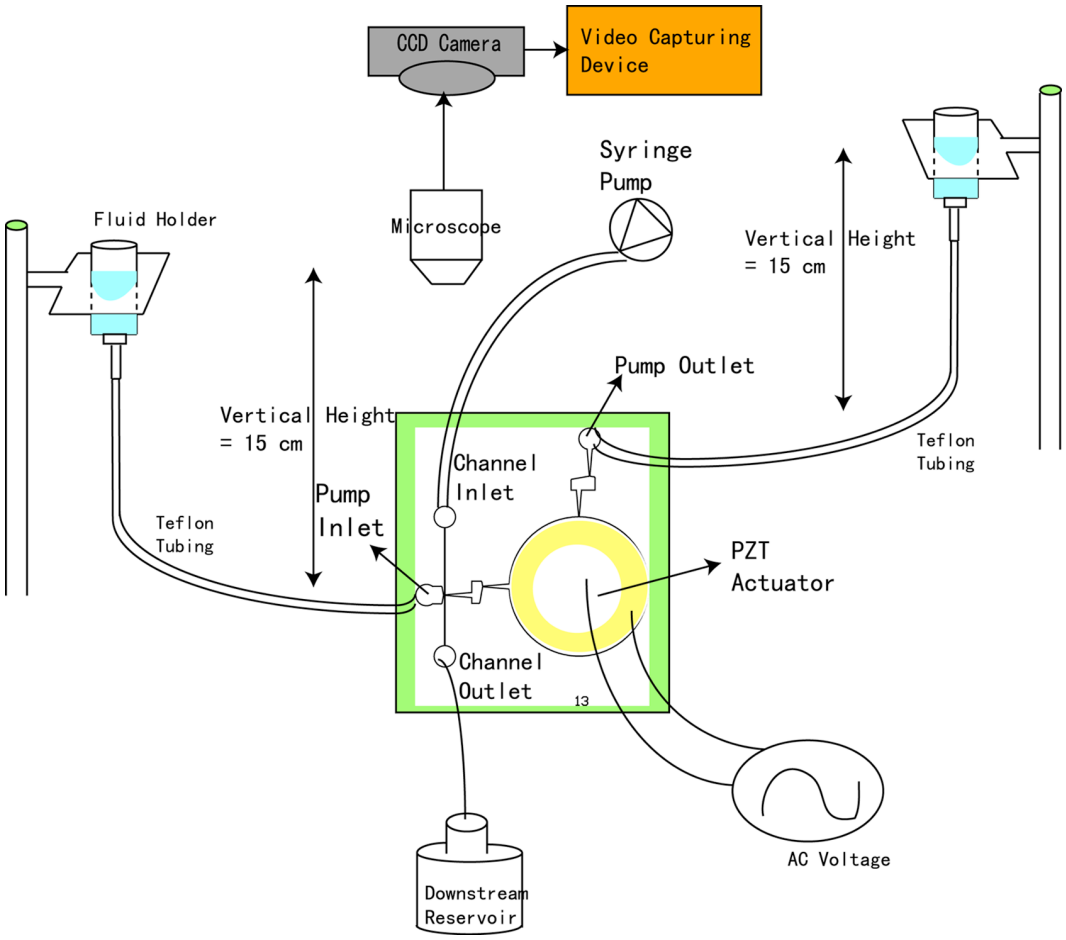

Figure 3.6 Schematics of experimental setup for particle sorting. Hydrodynamic pressure was imposed on the pump inlet and outlet by maintaining the height of the water column while fluidic flow is maintained by syringe pump.

To demonstrate sorting capability visually, individual air bubbles are introduced into the fluid inlet traveling at a speed of approximately 10 mm/s. During off state of the PZT actuator, the bubbles move directly down to the outlet of the main channel as expected from the simulation result. In contrast, as the PZT actuator is turned on (e.g. 50 Hz and 300 $V_{p\text{-}p}$ sinusoidal operation), the bubbles are redirected toward the right (e.g. toward actuation chamber), which again is consistent with the simulation result. The

frame-by-frame images in fig. 5 delineate the trajectory of one single sorted bubble. Bubbles of other sizes (~25-50 μm) have also been observed and followed similar trajectory. Limited by the 30 Hz frame rate of CCD camera, the periodic vibration behavior of the air bubble is not observed directly. However, the blurry boundary of the bubble in the direction of motion (Figs. 5b and 5c) is most likely caused by the periodic motion.

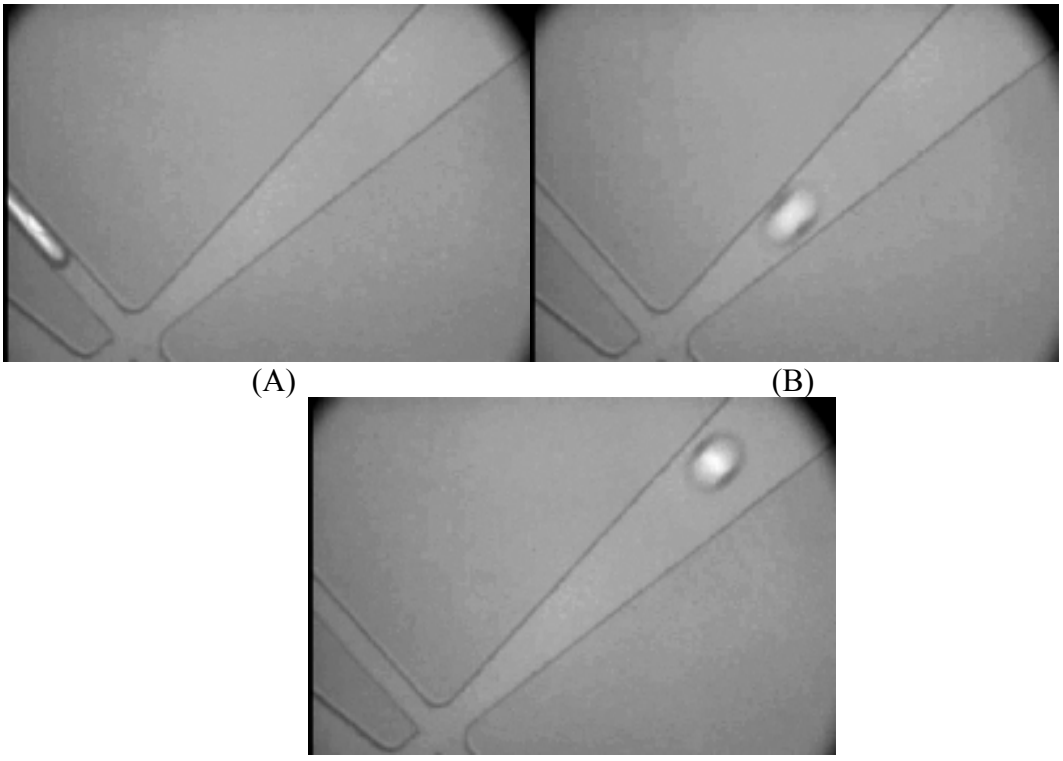

Figure 3.7 Sequential images showing the trajectory of the bubbles as the PZT actuator is active.

3.4.2 Bead Sorting Experiment

To investigate the sorting efficiency of the device, 5.8-μm polystyrene beads of ~4.4 x 10^5 beads/ml (Bangs Laboratories Inc., USA) are injected into the fluid inlet with average velocity controlled by the syringe pump. With the identical experimental setup described by fig. 4, experiment is carried out by monitoring the flux of beads exiting the outlet of the main channel. Since particles can either travel straight down to the outlet of the main channel or travel to the right toward diffuser outlet, counting beads exiting the main channel outlet over a given time interval (e.g. ~ 5 sec) allows us to quantify the sorting efficiencies of the device using the following relation:

$$\text{Sorting Efficiency} = \left(\frac{\chi_{off} - \chi_{on}}{\chi_{off}}\right) \times 100$$

χ_{off} and χ_{on} are the number of beads exiting the main channel when the PZT actuator is inactive and active respectively. This implies $\chi_{off} - \chi_{on}$ is the number of beads sorted into the diffuser. We monitor beads at the main channel outlet instead of at the intersection region because, near the intersection, the image of beads is blurred by the periodic motion, which renders bead counting very difficult. Also, as beads exit the outlet of the main channel, beads are decelerated. This allows easy and accurate visual counting.

Figure 3.8 shows the sorting efficiencies at different average particle speeds (determined by the imposed flow rate) for two different actuation frequencies. At relatively lower particle speed (~ 10 mm/s), sorting efficiencies above 95% are achieved. However, as the average particle speed increases, sorting efficiencies begin to decrease. As can be imagined, the fraction of total fluid being drawn into the diffuser

will become less as fluid gain higher downward momentum. Furthermore, because of the periodic flow excited by the PZT actuation, part of the fluid entering the intersection region will be drawn to the diffuser while another part will get pushed outwardly that eventually travels downward to the fluid outlet. However, this effect is negligible at low particle speed.

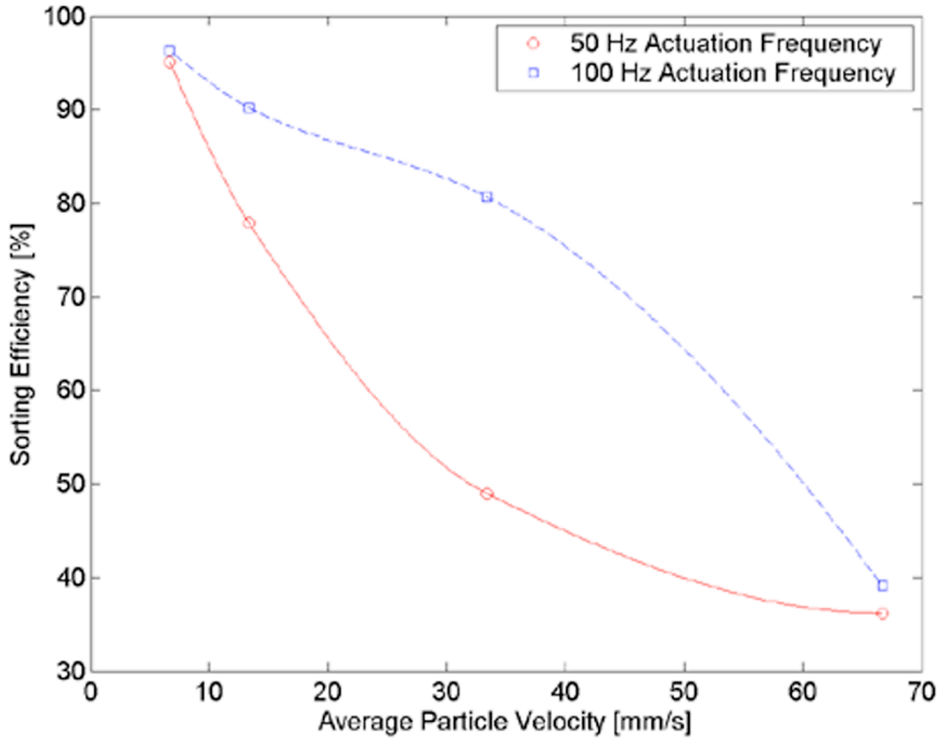

Figure 3.8 Sorting efficiency of the nozzle/diffuser as a function of particle's average velocity in the fluidic channel. The total number of particles counted for average velocities of 6.7, 13.3, 33.4, and 66.7 mm/s are 39, 200, 131, 204 for 50 Hz actuation and 36, 99, 198, and 205 for 100 Hz actuation.

As actuation frequency increases from 50 Hz to 100 Hz, sorting efficiencies at all particle speeds being investigated increase, and the amount of increase depends heavily on the particle speed. For example, comparing 100 Hz and 50 Hz actuation frequency, the sorting efficiency increases by 31% and 12% for particle speed of 13.3 mm/s and 33.4 mm/s, respectively. This can be explained by the increase in pumping flow rate at higher frequencies. The stand-alone nozzle/diffuser devices have pumping flow rates of 7.7 and 11 μl/min for 50 and 100 Hz actuation frequencies respectively. This is consistent with Gerlach's study [2] in which increase in actuation frequency below its resonance would increase the pumping flow rate of the nozzle/diffuser (i.e. sorting capability in our case). However, at high particle velocity (> 66.7 mm/s), regardless of its actuation frequency, nozzle/diffuser pump starts to lose its flow redirecting capability as fluid gains significant downward momentum.

3.5 Conclusion

In this chapter, we have demonstrated a cascaded nozzle/diffuser-based cell sorter on a PDMS substrate. Integration of PZT actuator pump is realized by the novel PDMS-to-Copper bonding technique, which permits optimal power transmission from Copper to water. Sorting is visualized by observing the trajectory of bubbles of various sizes during on/off actuation state of PZT actuator, and the results are consistent with our simulation. Moreover, 5.8-um beads are used to characterize sorting efficiencies at different average particle speeds as well as different actuation frequencies. The sorting efficiency can reach up to ~95%. In the future, actuation near resonant frequencies will be investigated to maximize the sorting efficiency and throughput.

References:

[1] E. Stemme and G. Stemme, "A valveless diffuser/nozzle-based fluid pump," Sensors and Actuators A, vol. 39, pp. 159-167, 1993.

[2] T. Gerlach and H. Wurmus, "Working principle and performance of the dynamic micropump," Sensors and Actuators A, vol. 50, pp. 135-140, 1995

[3] T. Gerlach, "Microdiffusers as dynamic passive valves for micropump applications," Sensors and Actuators A, vol. 69, pp. 181-191, 1998

[4] A. Olsson, G. Stemme and E. Stemme, "A numerical design study of the valveless diffuser pump using a lumped-mass model," J. Micromech. Microeng., vol. 9, pp. 34-44, 1999.

[5] O. C. Jeong and S. S Yang, "Fabrication and test of a thermopneumatic micropump with a corrugated p+ diaphragm," Sensors and Actuators A, vol. 83, pp. 249-255, 2000.

[6] C. Yamahata, F. Lacharme, and M. A.M. Gijs, "Glass valveless micropump using electromagnetic actuation," Microelectronic Engineering, vol. 78-79, pp. 132-137, 2005.

[7] S. Kar, S. Mcwhorter, S. M. Ford, and S. A. Soper, "Piezoelectric mechanical pump with nanoliter per minute pulse-free flow delivery for pressure pumping in micro-channels," Analyst, vol. 123, pp. 1435-1441, 1998.

[8] C. Yamahata, C. Vandevyver, and F. Lacharme, "Pumping of mammalian cells with a nozzle-diffuser micropump," Lab Chip, vol. 5, pp. 1083-1088, 2005.

[9] H. Andersson, W. Wijngaart, P. Nilsson, P. Enoksson, and G. Stemme, "A valve-less diffuser micropump for microfluidic analytical systems," Sensors and Actuators B, vol. 72, pp. 259-265, 2001.

[10] Y. Xia and G. M. Whitesides, "Soft lithography," Annu. Rev. Mater. Sci., vol. 28, pp. 153–184, 1998.

Chapter 4

Piezoelectric-actuated cell sorting module

Even though nozzle-diffuser based sorting module, as described in the previous chapter, is capable of sorting particles by flow re-direction at high efficiency, there are several limitations that cause the sorter inapplicable to perform high-thtoughput sorting down to single-cell level. To achieve flow re-direction, high input voltage (~ 300 V) is required and the fluid disturbance (e.g. periodic flow) caused by the actuation could alter the upstream flow pattern, making the timing of sorting difficult to predict. Also, at high particle speed, flow re-direction capability is severely undermined.

However, the insightful observation of the fluid displacement resulting from PZT actuation led us to modify the sorting mechanism. In this chapter, we describe a micro-sorter with a piezoelectric/metal bi-morphous actuator. Compared to other sorting mechanisms such as DEP [1-4], magnetic [5, 6] and hydrodynamic switching [7, 8] based sorting modules, the approach of the integrated PZT actuator offers several distinct advantages: 1) Simple fabrication process, 2) low voltage and low power consumption (<10 Vp-p and <0.1 mW), 3) precise control of the magnitude of transverse cell/particle deflection to enable single particle/cell sorting, 4) intrinsically much faster response (~0.1–1 ms) than conventional mechanical actuators (e.g. check valves and syringe pumps) or membrane valves.

4.1 Working principles

With a PZT actuator integrated on a chip, transverse displacement of fluid of the order of nanoliters can be introduced by the bending action (upward or downward) of the actuator controlled by the waveform of the input voltage (figure 4.1). As the targeted particle enters the sorting junction, the particle is being deflected transversely by the drag force of the displaced fluid and consequently follows the hydrodynamic fluid flow down to one of the collection channels. Without PZT actuation, unwanted particles travel straight down to the waste channel. To achieve the desirable amount of particle deflection, PZT actuator needs to provide a sufficient fluid volume displacement and a bending rate following the ramp of voltage. These needs are easily met in our system by adjusting input waveform and voltage magnitude for the PZT actuator.

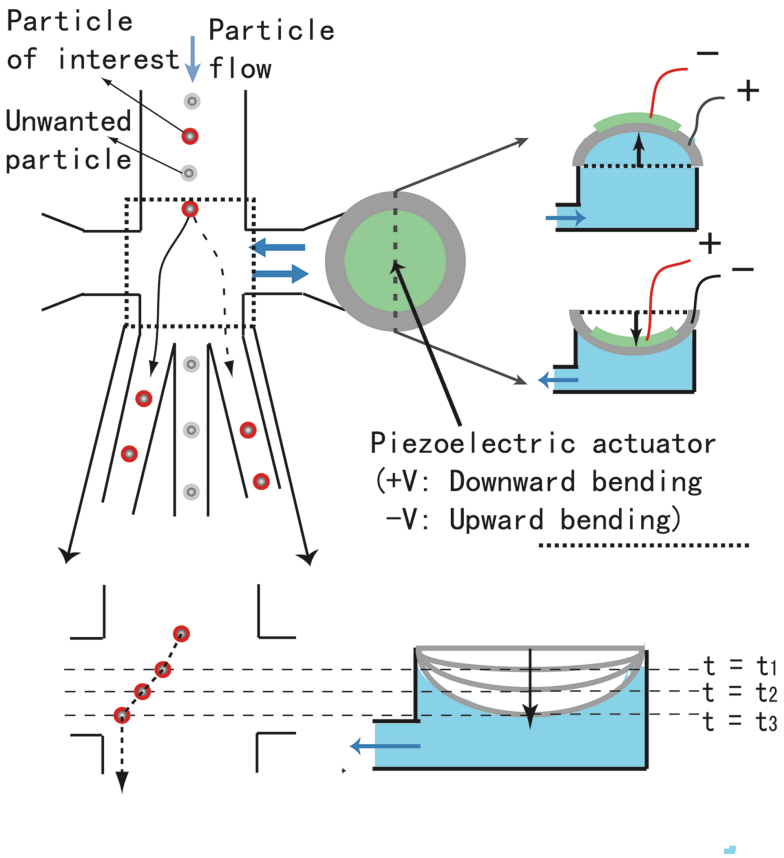

Figure 4.1 Operating principle of the piezoelectric (PZT) sorter. As particle enters the sorting junction, bending motion of the PZT actuator will temporarily disturb fluid flow (either to the right or left), causing particles to be deflected to the left/right channels. The bending orientation (e.g. upward or downward) and the amount of bending of the PZT actuator are controlled by the polarity and the magnitude of the input voltage, respectively. In the absence of PZT actuation, unwanted particles stay in the center streamlines, which travel straight down to the waste channel

4.1.1 Bead trajectory

4.1.1.1 Dynamic simulation

To visualize the trajectory of the particle subjecting to fluid deflection, a time-dependent simulation is conducted in Comsol 3.3 (Comsol Inc.). The dynamics of fluid flow is modeled using incompressible Navier-Stoke equation with water (with density = 1,000 kg/m^3 and viscosity = 1.002× 10^{-3}) as the fluid. The inlet velocity profile is assumed to be parabolic with maximum center velocity of 5 cm/s and the outlet channels assume atmosphere pressure. Transverse fluid deflection by the PZT actuation is modeled as time- dependent sinusoidal pressure at the boundary wall of the sorting junction while rest of the channel walls assume rigid and no-slip boundary conditions. At the sorting junction, pressure is defined as

$$P_{PZT\ boundary} = P_A \sin(2\pi ft) + P_o \quad (1)$$

P_A is the actuation pressure, t is time, f is the actuation frequency, and P_o is the hydrodynamic pressure established by the flow. To see the effect of PZT actuator-induced flow response, 5-μm particles are released into the center of the flow stream at a velocity of 5 cm/s and the movements of the particles are modeled using Khan and Richardson's force [9]. Time-dependent boundary parameters, P_A, f, and P_o, are set at 1.5 kPa, 250 Hz, and 0.63 kPa respectively.

4.1.1.2 Experimental bead trajectory

To visualize experimental particle trajectory, the device is mounted on a high-speed camera attached microscope stage. The particles (5-μm polystyrene beads) are introduced into the device using syringe pumps (1:10 sample to sheath flow) and PZT

actuator is driven by a function generator (Tektronix Inc.) under operation conditions of 250 Hz and 9 V_{p-p}.

The dynamic simulation shows the trajectory of a 5-μm bead subjecting to a time-dependent sinusoidal pressure at the right boundary wall (Figure 4.2 (b), (d), and (f)). As the particle reaches the sorting junction at a velocity of 5 cm/s, the pressure force deflects the flow pattern, which in turn carries the particle down to the left collection channel. Particles released at other times (not shown here) can follow different trajectories (e.g. deflected to the right channel or to the center channel) since they experience different pressure force depending on the time they enter the sorting junction. To verify the bead trajectory experimentally, 5-μm polystyrene beads are used. Figure 4.2 (a), (c), and (e)) show how the single bead moves (~5 cm/s) when subjected to PZT actuator-induced fluid disturbance. Similar to the simulation result, as the PZT actuator bends down, the flow imposes a drag force on the bead to deflect the bead off the center stream to the left channel. Also, as the PZT actuator is turned off, the particle immediately resumes its undisturbed trajectory (down the center channel). The result shows that the sorter can impose sufficient drag force to alter particle trajectory in a predictable manner. Furthermore, it shows the promise that the sorter can sort single particles at relatively high speed under low power consumption (<0.1 mW).

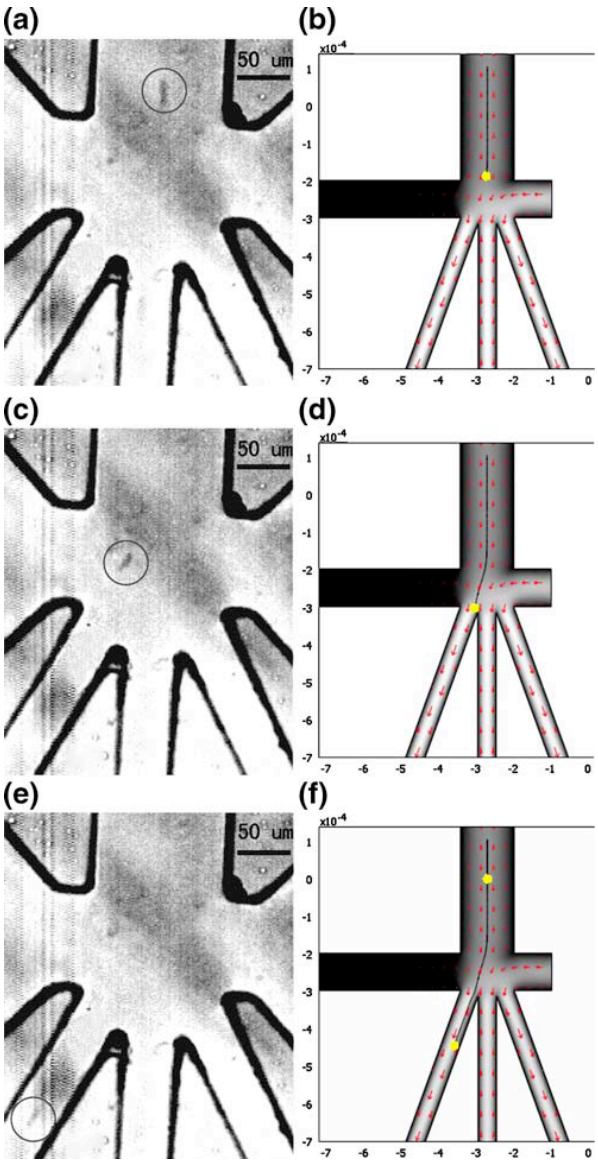

Figure 4.2 Sequential images showing particle trajectory based on (b), (d), and (f) dynamic simulation results (time stepping of 1.5 ms) and (a), (c), and (e) experimental results (images taken at 0, 1.3, and 3.3 ms). The simulation is done by applying 250 Hz sinusoidal dynamic pressure (~1.5 kPa) to the sorting junction, and the experiment is carried out under 250 Hz (e.g. sinusoidal) and 9 V peak-to-peak PZT actuation. Sorted bead is marked for clarity

4.2 Device fabrication

The device is fabricated using the conventional micro replica molding technique in which device features are photolithographically defined by SU-8 photoresist mold (figure 4.3(a)) and then transferred to a polydimethylsiloxane (PDMS) substrate. For device assembly, the PDMS substrate and glass are surface treated in UV ozone chamber (Jelight Inc., Irvine) with a lamp output of 28 mW at 254 nm. Bonding occurs as they are put into physical contact. For the subsequent PZT actuator and PDMS substrate bonding, the mechanically polished stain- less steel surface of the PZT actuator is exposed to UV ozone treatment for 10 min. After the actuation chamber of the PDMS substrate (Sylgard 184, Dow Corning) is created using a 16-mm diameter punch, both the PDMS substrate and the PZT actuator are UV ozone treated for another 5 min. Immediately after the UV o-zone treatment, the stainless steel surface of the PZT actuator is aligned to the PDMS actuation chamber and put in contact with the PDMS substrate for bonding. The bonding process is completed after the sample is baked at 85°C for 8 h (Fig. 4.3(b)). For the last step of device fabrication, Teflon tubings are inserted into the inlets and outlets of the device for fluid flow introduction. The device (Fig. 4.3(c)) is then primed using vacuuming filling under −30 inch Hg. The strong stainless steel-to-PDMS bonding prevents fluid leakage and optimizes power coupling from the PZT actuator to the fluidic channels.

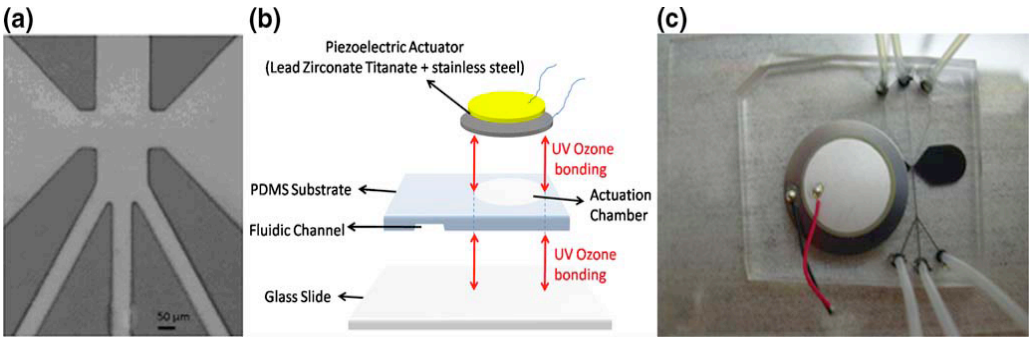

Figure 4.3 (a) The device features consist of one 150 µm x 50 µm main channel and three 50 µm x 50 µm collection channels. The opening of the nozzle (perpendicular to the flow) is 100 µm wide. (b) Device fabrication involves two successive bonding using UV-ozone treatment. The resultant device is shown in (c)

4.3 Characterization of PZT-actuated sorting module

4.3.1 Frequency response

To characterize fluidic response, 5 mM of Rhodamine 6G is introduced to the sample channel and hydrodynamically focused (1:10 sample to sheath flow). Once the fluid flow is stabilized, the PZT actuator is electrically modulated and the behaviors of stream under various voltages and frequencies are analyzed by using the high-frame rate CCD at 6,000 fps.

Flow switching of the focused rhodamine stream can be observed under PZT actuation. As PZT actuator pushes the fluid to the left under a rising bias voltage, the rhodamine stream temporarily gets deflected towards the left channel (Fig. 4.4(a)). Similarly the stream is temporarily shifted towards the right channel as a falling voltage

is applied to the PZT actuator (Fig. 4.4(c)). Without actuation, the stream travels directly down to the center channel (Fig. 4.4(b)). Such controlled flow switching behaviors are observed at high actuation frequency up to ~1.7 kHz (at 20 Vp-p). The upper limit of the switching frequency has not been experimentally determined yet. However, the channel geometry has been optimized to minimize the viscous effect when subjecting to fluid movement. In order to find out the maximum sort rate at single particle level, further theoretical analysis needs to be investigated to determine the limit of flow response under actuation. Nonetheless, the current study shows that the design can potentially sort several thousand particles/cells per second at single particle/cell resolution.

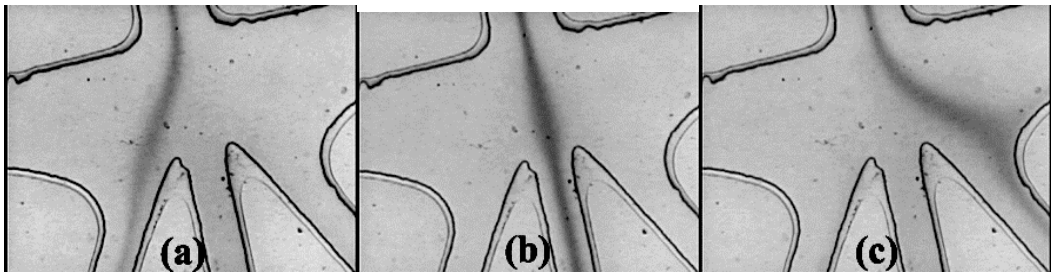

Figure 4.4 Images showing deflection of rhodamine dye as a result of PZT actuation. (a) The rhodamine stream switches to the left as the PZT disk bends downward. (b) no stream deflection when the PZT actuator is off. (c) The rhodamine stream is deflected to the right channel as the PZT disk bends upward.

To visualize whether particles/cells can be manipulated at specified frequencies, we introduced an *e. coli.* sample (~7×10^5 cells/ml) to the device and image the manipulative effect of PZT actuation. At 20 Hz, 3 Vp-p actuation, we analyze the E. Coli. cells that are being deflected into the left and right channels. At a low flow rate of

~2 μl/min, a sorting throughput of 24 cells/s is recorded. To increase the sorting throughput, we increase the total flow rate to 18 μl/min, corresponding to a travel speed of ~6 cm/s for cells in the center stream, as well as the actuation voltage and frequency to 5 Vp-p and 200 Hz. At this flow rate, the *E. Coli.* cells pass through the sorting junction (~100 μm in length) in 1.7 ms. Figure 8 shows the *E. Coli.* cell deflection result in the aforementioned experimental conditions. Individual peaks represent single cells entering the right/ left collection channels at the specified times. With frame- by-frame analysis, we determine the cell deflecting rate to be 330 cells/s. Notice that all the red peaks occur within the rising cycle of the applied voltage, representing samples entering the left channel. Similarly, all the blue peaks occur within the falling cycles of the applied voltage, representing samples entering the right channel. This is in total agreement with the proposed sorting mechanism that a rising (falling) voltage bends the PZT downward (upward) to create a transient transverse flow towards the left (right) channel, which in turn directs the cells into the desired collection channel.

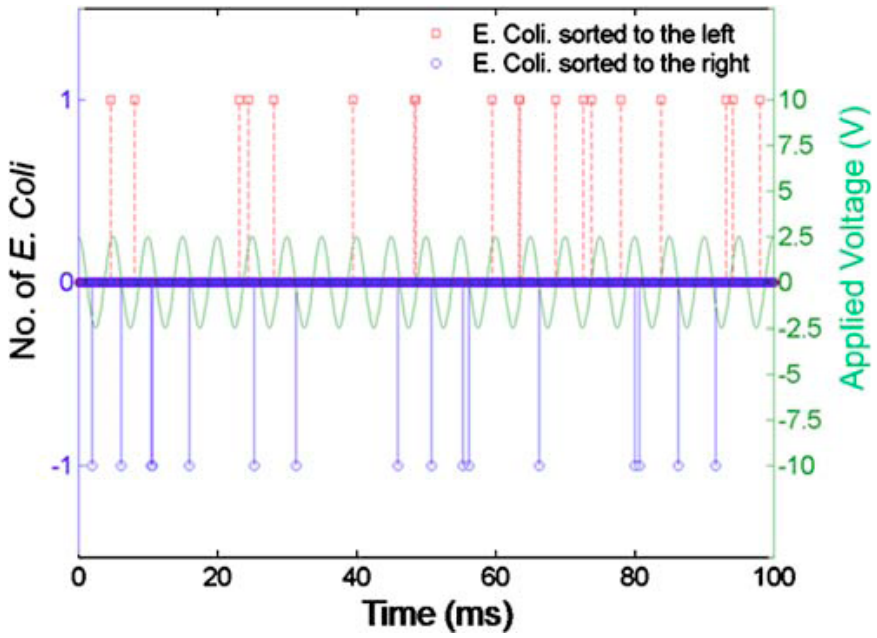

Figure 4.5 Deflection of single E. Coli. cells at 200 Hz frequency and 5 Vp-p actuation voltage. The peaks are obtained by identifying cells visually as they are sorted to the left/right channels. Approximately 18 and 17 *E. Coli.* cells are sorted to the left/right in 100 ms in this case. However, a total of 330 cells are visually counted in 1 sec. Note that the cells that are sorted to the left/right all fall into downward/upward (bending down/up) ramping state of the PZT actuator, in good agreement with the theory. Also note that few rare peaks that appear denser mean that two cells can exit a particular collection channel at roughly the same time.

4.3.2 Response of input voltage

To manipulate flow precisely, it is also essential to characterize the magnitude of deflection resulted from PZT actuation since sorting optimization requires sufficient deflection. To characterize deflection magnitude, 10-μm beads are introduced into the

device at a velocity of ~ 10 cm/s. Due to the high particle speed, a high-frame rate CCD is used to capture deflection behavior as a function of PZT actuation voltage. Figure 4.6(A) depicts the experimental trajectory of a 10-μm bead at the sorting junction. The processed image is consisted of 11 consecutive images at 0.3 ms apart from each other. Determination of deflection magnitude as a function of different input voltages is done by visualization while changing PZT input voltages. Figure 4.6(B) reveals the resulting particle trajectories subjecting to different input voltages. Amount of deflection is measured from the center of the sample channel to the outermost location where the deflected particle stops in the transverse direction (perpendicular to the flow). The result is summarized in figure 4.6(C). The estimated minimum voltage to induce sufficient particle deflection for sorting is ~ 3 V. However, the estimated voltage does not imply the value is the optimized sorting voltage. The reason is that lower deflection implies the timing of the sorting has to be very precise to guarantee successful sorting. Thus, before determining the actuation voltage, it is desirable to assess the biological mixture at hand. If the targeted sample is very rare, higher deflection is preferred since it increases the chance of successful sorting. In contrast, if the purity of the sorted sample is essential, lower deflection actuation should be used since this operation minimizes chance of sorting unwanted samples.

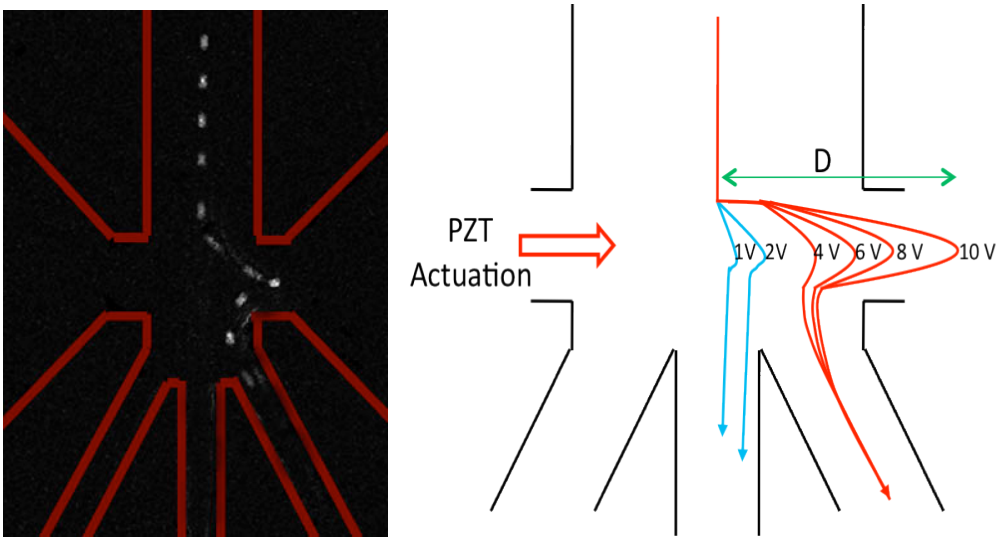

(A) (B)

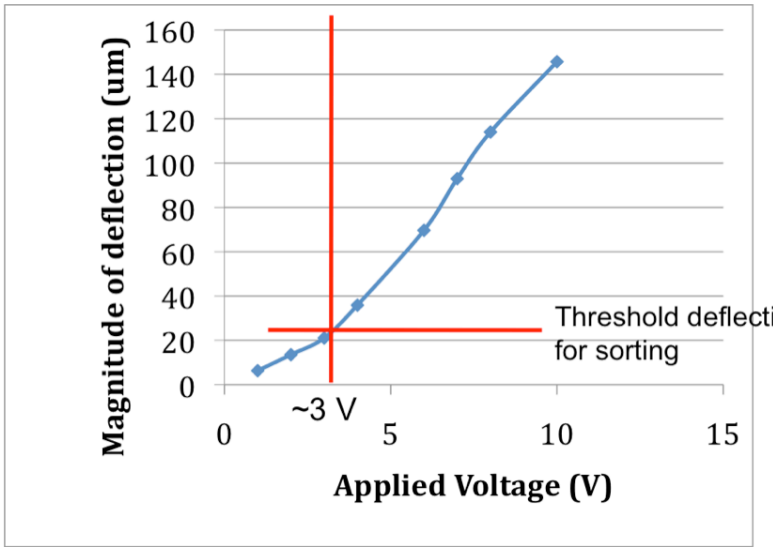

(C)

Figure 4.6 Characterization of deflection magnitude. (A) Trajectory of a 10-μm bead as a result of PZT actuation: Image showing 11 superimposed images with every image taken 0.3 ms apart. (B) Schematics and (C) a plot showing magnitude of deflection (with reference point at the center of the channel) at different input voltages. The estimated threshold voltage for sufficient deflection for sorting is ~ 3 V.

4.4 Conclusion

We have demonstrated, for the first time, a microfluidic cell sorting module with integrated piezoelectric actuator. The device is easy to fabricate and operates at less than 10 V_{p-p}. Both simulation and experiment show that particles of any size, shape, and density of interest can be individually sorted in a controlled manner. In the experiment of instantaneous flow switching, we have shown that the flow stream responds to the piezoelectric actuator at high frequency (~1.7 kHz) and the amount of deflection of cells/particles in the flow can be precisely controlled. In the experi- ment of E. Coli deflection, a sinusoidal voltage deflects cells at a rate of 330 cells/s and shows a highly repeatable operation consistent with the theory. Characterization of magnitude of deflection experiment showed that the minimum voltage needed to cause sufficient deflection is ~ 3 V. In summary, the sorting module is inexpensive, easy-to-fabricate, and can deflect particles at high rates (response time of ~ 0.1 – 1 ms). Due to these characteristics, the proposed sorting module can be used for high-throughput (e.g. rare-event sorting) sorting with the incorporation of detection and electronics systems, which will be discussed in next chapter.

References:

[1] B. H. Lapizco-Encinas, B. A. Simmons, E. B. Cummings, and Y. Fintschenko, "A valveless diffuser/nozzle-based fluid pump," Electrophoresis, vol. 25, pp. 1695-1704, 2004.

[2] S. Fiedler, S. G. Shirley, T. Schnelle, and G. Fuhr, "Dielectric sorting of particles and cells in a microsystem," Anal. Chem., vol. 70, pp. 1909-1915, 1998

[3] I. Doh and Y.-H. Cho, "A Continuous cell separation chip using hydrodynamic dielectrophoresis (DEP) process," Sensors and Actuators A, vol. 121, pp. 59-65, 2005

[4] X. Hu, P. H. Bessette, J. Qian, C. D. Meinhart, P. S. Daugherty, and H. T. Soh, "Marker-specific sorting of rare cells using dielectrophoresis," PNAS, vol. 102, pp. 15757-15761, 2005.

[5] N. Pamme and C. Wilhelm, "Continuous sorting of magnetic cells via on-chip free-flow magnetophoresis," Lab Chip, vol. 6, pp. 974-980, 2006.

[6] N. Pamme and A. Manz, "On-chip free-flow magnetophoresis: continuous flow separation of magnetic particles and agglomerates," Anal. Chem., vol. 76, pp. 7250-7256, 2004.

[7] J. Kruger, K. Singh, A. O'Neill, C. Jackson, A. Morrison, and P. O'Brien, "Development of a microfluidic device for fluorescence activated cell sorting," J. Micromech. Microeng., vol. 12, pp. 486-494.

[8] A. Wolff, I. R. Perch-Nielsen, U. D. Larsen, et al. "Integrating advanced functionality in a microfabricated high-throughput fluorescent-activated cell sorter," Lab Chip, vol. 3, pp. 22–27, 2003.

[9] J. M. Coulson, J. F. Richardson, J. R. Backhurst, J. H. Harker, Chemical Engineering, 2nd edn Butterworth-Heinemann Ltd, Oxford, pp. 970, 1982.

Chapter 4 or portion thereof has been published in ***Biomedical Microdevice,*** **Vol. 11, Iss. 6, pp. 1223-1231** and ***Lab Chip*****, Vol. 10, pp. 1567-1573.**

Chapter 5

System integration of the piezoelectric-actuated micro-fabricated fluorescence-activated cell sorter (μFACS)

Having developed a low-cost, lower-powered, and fast-response piezoelectric sorting module, we are now able to develop a sensitive detection platform as well as a robust closed-loop control system that enables high-throughput sorting of biological agents. The system integration developed in this chapter is consisted of 3 main components: 1) on-chip excitation using optofluidic waveguide, 2) piezoelectric-actuated cell sorting module, and 3) a spatial filter-modulated light collection system

with pre-programmed real-time electronics control system (figure 5.1). In addition to the benefits offered by piezoelectric actuation, the developed detection strategy (1) and 3) from above) offers several distinct advantages over other μFACS systems including detection at multiple points, real-time signal amplification, and real-time sorting verification. Thus, in this chapter, I will show how the μFACS system can be used to sort mammalian cells at high-efficiency, high-throughput, and high sample enriching capability.

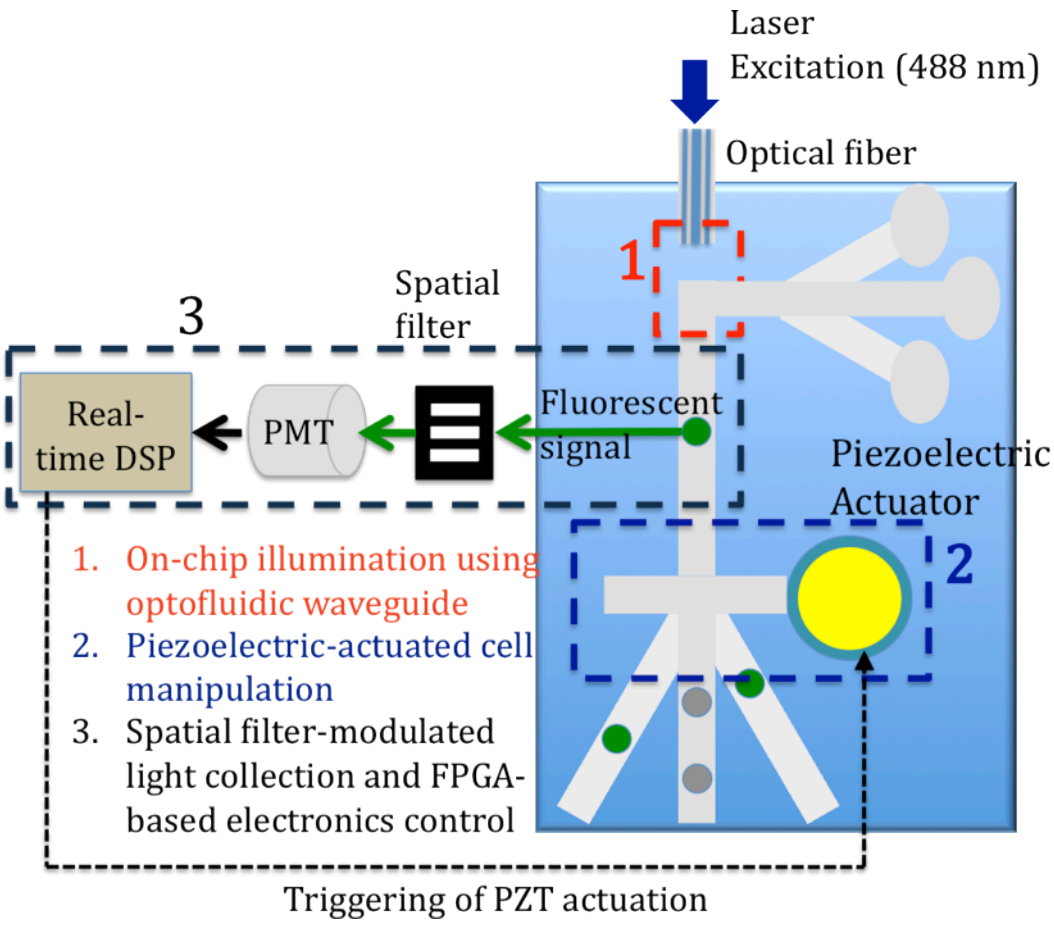

Figure 5.1 μFACS platform using on-chip light illumination, on-chip piezoelectric actuation, and off-chip spatial filter-modulated light and electronics control system.

5.1 The architecture of the integrated μFACS

5.1.1 Optofluidic waveguides

On-chip excitation using optofluidic waveguides is an attractive light illumination method because since fluidic channels and optical waveguides are photolithographically defined, it eliminates the need for precise optical alignment. A number of research groups have shown that fluidic channels and waveguides can be fabricated on the same substrate for light illumination [1-3] and bio-imaging [4]. Recently, Cho et. al. [5] have developed a optofluidics-based light illumination method that is compatible with μFACS system using Teflon-AF coating. Because PDMS (substrate material for μFACS) has a index of refraction of ~ 1.41, it is essential to coat a material on the PDMS channel that has a refractive index less than PBS/water (n ~ 1.33) to ensure light guiding (through total internal reflection). With Teflon-AF coating, light can be guided directly into the sample fluidic channel for direct illumination (light travels in parallel with analytes). Thus, the method enables detection at multiple points along the sample path, which serves as the basis for real-time sorting event verification that will be discussed later.

5.1.2 Fluorescence collection using encoded spatial filter

To perform fluorescence-activated cell sorting, a closed- loop control system is built (Figure 5.2). A 40 mW 488 nm laser diode is employed as the excitation source. The specially designed spatial filter allows fluorescence from specific locations in the channel to reach the photo- multiplier tube (PMT) detector. Afterwards, the fluorescent

emission signal from the cell/particle being sorted is amplified. Once a threshold is reached, a time-delayed actuating signal will be sent to drive the actuator, triggering the sorting action.

A spatial filter allows only fluorescence from certain areas in the channel to reach the detector, thus cutting down the background and crosstalk. Using specially designed patterns, one can spatially encode a fluorescent signal and then transform the signal into a temporarily encoded signal as the targeted particle/cell travels at a speed. We use photolithographic transparency masks (Cad/art services, Inc.) to create spatial filters. The spatially encoded patterns have triple slits and double slits. The former encodes the detection signal and the latter the verification signal from the particles/cells sorted into the designated channel. The width of the slits is 0.25–0.5 mm, translated to 12.5–25 μm on the microfluidic channels before magnified by a 20x microscope objective (Figure 5.3).

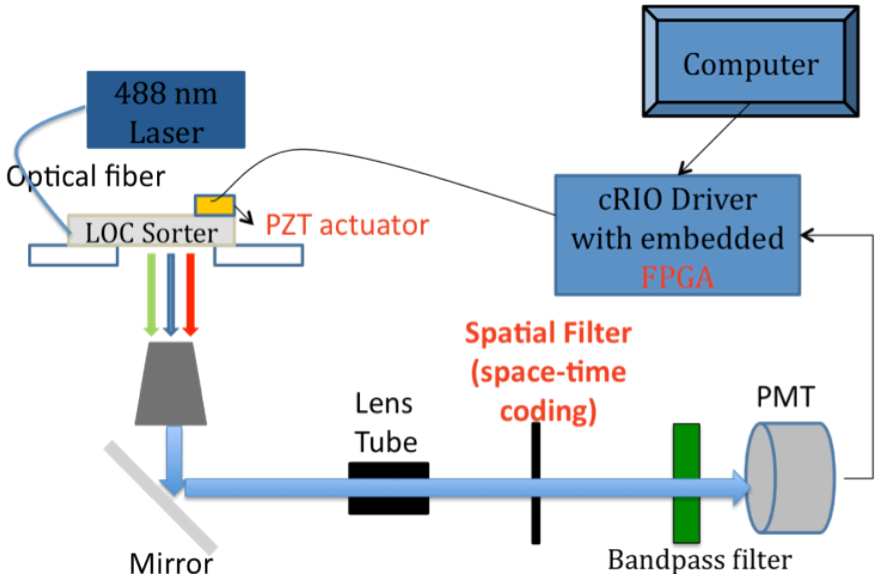

Figure 5.2 Experimental setup of the μFACS system

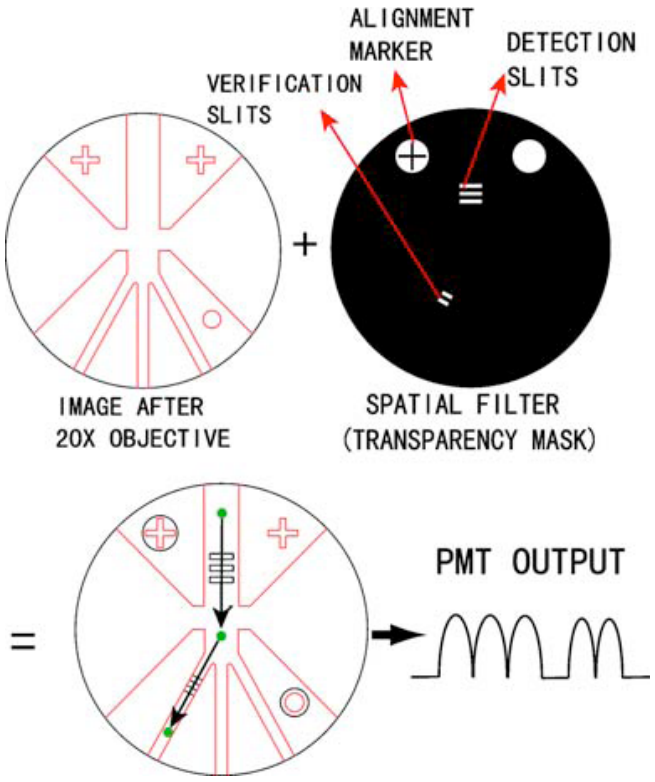

Figure 5.3 Spatial filter is designed to purpose- fully coincide with the image plane after magnification. As fluorescent particle passes through detection slits and gets sorted down to the verification slits, the PMT detector is expected to register signals of 3 peaks followed by 2 peaks.

5.1.3 Real-time electronics control algorithm

Real-time electronic control is programmed using Lab- view (National Instrument) with a programmable external driver (CompactRio, NI). The external driver has an independent operating system with an embedded field- programmable gate array (FPGA) chip. The measured jitter of the system is <10 μsec. The flow of the electronic control is shown in Fig. 5. The random high pulse noises of PMT (e.g. caused by sporadic discharge of the device) are removed before running the signal amplification

algorithm based on finite impulse response (FIR) filtering. With an FIR matched filter, the signal-to-noise (SNR) ratio can be increased by 18 dB. After SNR enhancement, threshold and search of maximum signal criteria are applied to determine the presence of the detected particle. A signal above threshold indicates that a particle/cell to be sorted is found, triggering the following actions: (a) a delay counter delays the firing of the pulse generator, (b) a preprogrammed output voltage signal is fired to drive the PZT actuator, (c) at certain time period the system is ready to detect the "verification" signal from the sorted sample travelling through the "verification zone", and (d) update record of the sorting efficiency and sorting error. The amount of time delay equals the travel time of the particle from the optical detection zone to the sorting junction. Until the sorted particle is verified, the PZT actuator will not be fired again. This avoids the problem of confusing the verification signal with the signal of particles traveling too close to the particle being sorted.

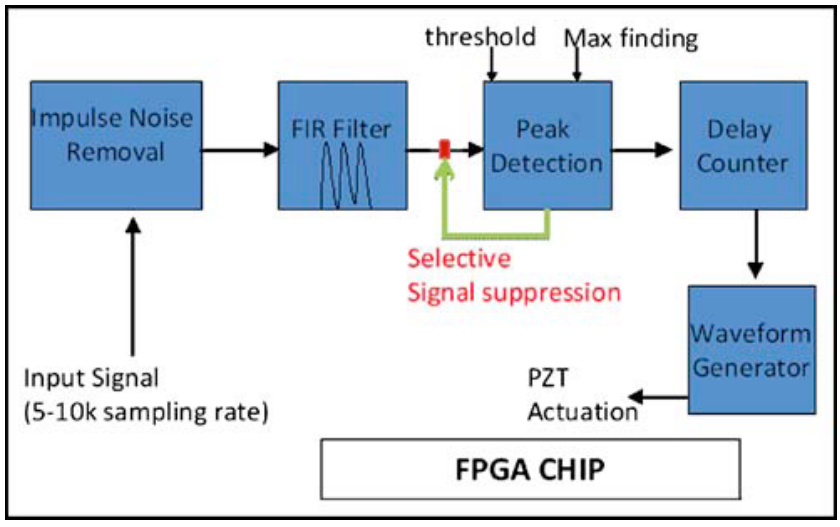

Figure 5.4 Flow chart showing the process flow of the electronics control algorithm. The algorithm is programmed into the FPGA chip embedded in the external driver.

5.1.4 Signal amplification and sorting verification

With the encoded spatial filter incorporated into the μFACS system as shown in figure 5.3, signal amplification and sorting event verification could be achieved simultaneously using the real-time DSP processing. As a 10-μm fluorescent bead crosses the detection slits and is sorted to pass the verification slits, a 3-peak signal followed by a 2-peak signal are observed (Figure 5.5). The distinctive nature of the peaks allows real-time monitoring of sorted and unsorted particles, which, to our best knowledge, has never been implemented in any μFACSs. The detected signals can be amplified using a real-time signal processing algorithm based on the concept of match filter. The mathematical model of the FIR match filter can be described as

$$Y[n] = \Sigma^{M}_{k=0} b_k \cdot x[n - k] \qquad (1)$$

where Y[n] is the output signal, x[n] is the input signal, b_k is the filter coefficients, and M is the filter order, which specifies the number of taps (e.g. M+1) for the filter coefficients. Thus, in the proposed design, the match filter coefficients, which assume the shape similar to the detected signals (e.g. 3 sinusoidal lobes), are used to convolve with the detected signal, resulting in SNR enhancement of ~18 dB, as shown in Figure 5.6.

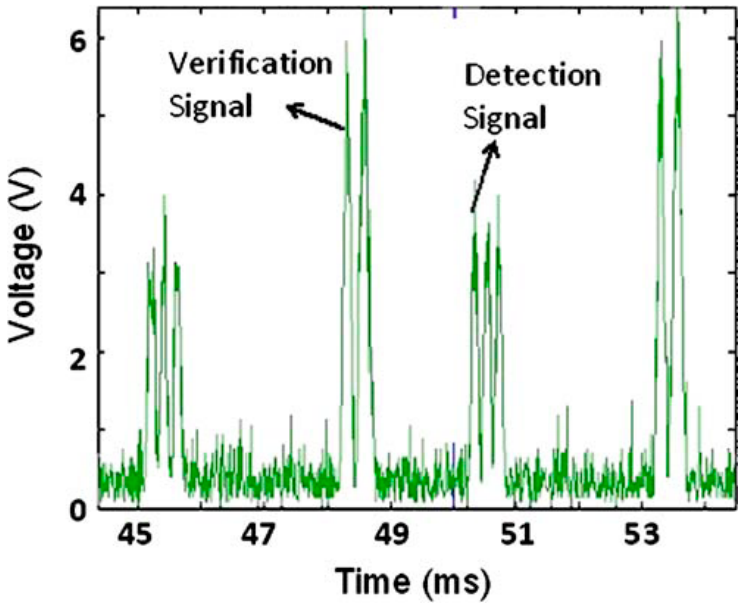

Figure 5.5 Raw signals of 10-μm beads passing through the 3-slit upstream detection zone and 2-slit downstream verification zone. Every peak results from particle passing through individual slits (slit width = 17.5 μm). Note that for the two particles shown here, the time for them to travel from the detection region down to the verification region is ~2 ms.

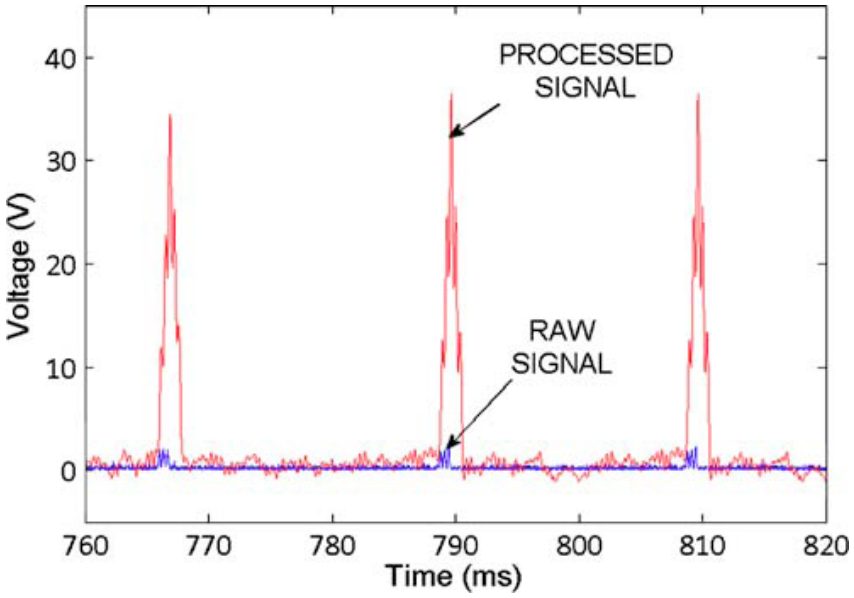

Figure 5.6 A comparison between raw and amplified signals with FIR match filter. The amplified signal shows a sensitivity enhancement of ~18 dB

5.2 Characterization of sorting efficiency

To characterize the sorting efficiency, 10-μm fluorescent beads (Bangs Laboratory) with a concentration of ~1×10^5 particles/ml and excitation/emission wavelength of 480/520 nm are used. The beads are hydrodynamically focused under a sample-to-sheath flow ratio of 1:5 with velocities of ~8 cm/s. Sawtooth pulses of 10 Vp-p (1.5 ms pulse width) are used to drive the PZT actuator. The delay time (~1.5 ms) is estimated according to the velocity of the particle. The measurement data are recorded for a total period of 10 s. We use the setup to measure the sorting efficiency and the sorting error. The former refers to the success rate of a voltage pulse to direct the targeted particle into the designated channel; and the latter refers to the possibility for an unintended particle to enter the designated channel by mistake. A sorting efficiency less

than 100% could be due to non-ideal timing control and velocity variation due to lack of 3-dimensional flow focusing. In most practical applications, this is less a concern than sorting error. On the other hand, a sorting error, caused likely by non-ideal flow disturbance due to actuation, could have a much more adverse effect. Therefore, a strategy is taken to achieve the lowest possible sorting error at some expense of sorting efficiency. From a subset of the measurements, Fig. 11 shows a sorting efficiency of ~84%. Other measurements consistently show similar results (84% ± 5%). The distinction between successfully and unsuccessfully sorted particles is by examining the presence and absence of the verification signal following the first detected signal. The verification signal is designed to have a lower intensity than the first detected signal because the spatial filter for the verification signal has only two slits, producing a less match to the triple-peak FIR filter. Nonetheless, the amount of SNR enhancement for the verification signal still allows clear identification. In the instance that two particles are spaced closely such that the second particle enters the detection region before the first particle is being verified downstream, to avoid misfiring of PZT actuation due to cross-talking between detection and verification signals, our algorithm is set up to keep the actuator inactive until the first particle is sorted and verified. This holding period (~3–4 ms) also contributes to the reduced sorting efficiency. From the data in figure 5.7 and a series of preliminary measurements, we have achieved 0% sorting error and the estimated minimum particle spacing to ensure error-free sorting is ~100 μm.

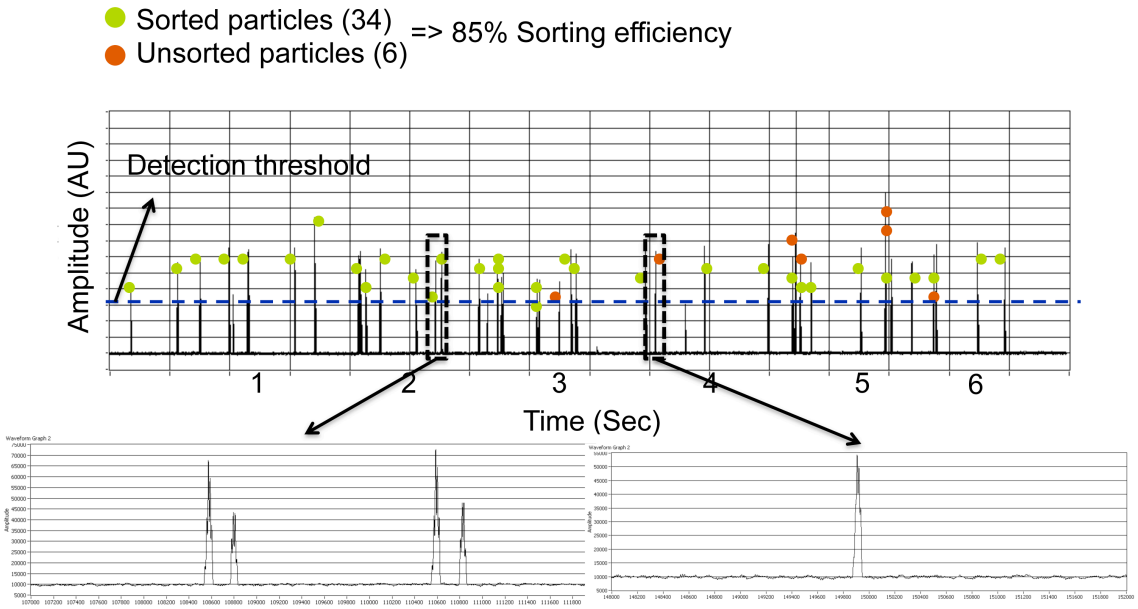

Figure 5.7 Sorting efficiency and sorting error characterization. 34 beads (blue dots) out of 40 detected fluorescent beads have been successfully sorted, resulting in ~84% sorting efficiency. For every single sorted particle, the detected signal (upstream) is always followed by a verification signal (e.g. larger peak followed by a smaller peak). In contrast, the absence of verification signals results in particles not being sorted. In this experiment, there is 0% sorting error since no particles have been falsely sorted.

5.3 Characterization of sample enriching capability

5.3.1 Bead sorting

To quantitatively determine the performance of the integrated μFACS, 10 μm fluorescent polystyrene beads (Bangs Laboratory Inc., USA) are mixed with non-fluorescent 5-μm beads at an initial mixture ratio of 0.0067 (~ 1:160 as determined by a commercial FACS machine – FACScan, BD, USA) and a concentration of 1 x 10^7

beads/ml. The sample and sheath flowrates are set at 5 μl/min and 50 μl/min, respectively. Utilizing the aforementioned space-time coding technique (e.g. signal detection and sorting verification), sorting parameters that are programmed to drive the PZT actuator can be optimized in the first few minutes of experiment, resulting in significant savings in sample volume. After parameter optimization, the verification slits are physically blocked by a piece of black paper (place right in front of the verification slits) minimizing interference between verification and detection signals.

After continuous automated sorting for ~30 min with the optimized sorting parameters, the sorting result shows a 200-fold enrichment at a throughput of 1500 beads/sec (Figure 5.8). The result from run to run is very consistent under the same flow conditions and sample preparation. The output mixture ratio between the 10 μm fluorescent beads and the 5 μm non- fluorescent beads is about 1.3:1 after sorting while the initial ratio is 1 : 160. The output mixture ratio implies that some unwanted 5 μm beads are sorted accidentally even though the 10 μm beads are significantly purified. This occurs because the velocity of the beads is not constant due to the lack of 3D (vertical direction) flow confinement. This causes an error in defining the proper timing for triggering the actuator, occasionally deflecting both the wanted and unwanted beads into the target channel. Given the velocity of the beads (5–7 cm/sec) and the initial concentration (10^7 beads/ml), the average distance between two beads is about 50–80 μm, which implies the possibility of accidentally sorting two cells in one actuation since the nozzle opening at the sorting junction is 100 μm wide.

To determine the mixture ratio contents (beads or cells), it is desirable to use the conventional gold standard FACS machine. Thus, once the sorted mixture is collected, it is immediately transferred to a commercial FACS (FACScan, BD Biosciences) for purity analysis. To determine proper gating, a portion of the initial mixture is analyzed prior to sorted mixture. Gating by forward scattering (FSC) signals is used to determine total sample population. With the same gating, fluorescein histograms (FITC) of both the initial and the sorted mixtures are analyzed to determine the respective mixture ratios and, therefore, the enrichment factor. This FACS validation method is also used for sorting of mammalian cells, which will be discussed next.

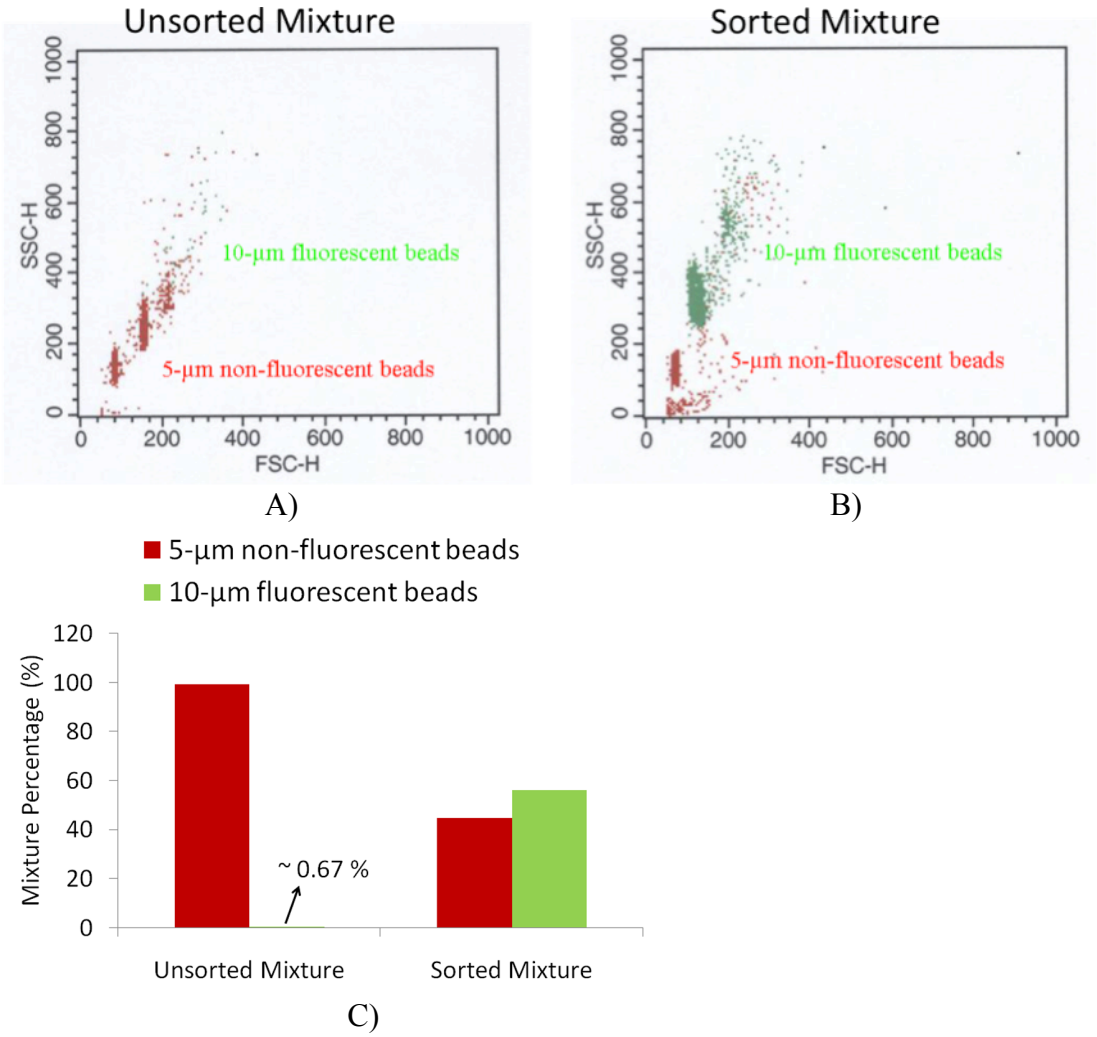

Figure 5.8 Scattering plots shows the result of the A) initial and the B) sorted sample mixtures. Green/red dots represent fluorescent 10-µm/non-fluorescent 5-µm bead signals. C) The population ratio of the initial bead mixture is 0.67:100. After sorting for 30 min, the mixed ratio becomes 1.3:1, yielding an enrichment factor of around 200.

5.3.2 Sorting of human mammalian cells

To validate the sorting capability for biological applications, a mixture of stained and non-stained K562 cells (human erythroleukemic cell line) was used. The fluorescent

cells were prepared by incubation in 2 μM carboxyfluorescein diacetate succinimidyl ester (CFSE) in PBS/BSA at 37 C for 15 min. After washing, the cells were incubated at 37 C for another 15 min. Following a second washing step, the stained cells are mixed with non-stained cells at an initial mixture of 0.0081 (determined by the commercial FACS) at a concentration of 1.1 x 10^7 cells/ml. Before introduction to the μFACS device, the cells are filtered through a 40-μm cell strainer (BD Bioscience, USA) to remove large cell clumps. FACS fluid (BD Bioscience, USA) was used as sheath fluid for both aforementioned samples.

Under similar flow conditions (e.g. bead sorting), sample concentration, and initial mixture ratios, flow cytometric analysis shows an enrichment factor of 230 fold (Figure 5.9), which is the highest value ever demonstrated in μFACS systems. Based on the sample flow rate (6 μl/min) and cell concentration (1.1 x 10^7 cells/ml), a throughput of 1000 cells/sec is achieved. Even though the sample concentration is relatively high compared to conventional flow cytometric analysis (10^6–10^7 cells/ml), no significant cell stiction is observed due to the chemically inert Teflon AF coating. Cell clogging, which is common among μFACS systems, can greatly compromise sorting purity as well as the ability to collect sufficient targeted cells because the device becomes unusable as the clogged cells block the fluid flow. Owing to its minimized clogging, the proposed system can sustain continuous operation for long periods of time (>2 h). This is essential for sorting of rare cells such as stem cells and circulating tumor cells. By continuous operation at >1000 cells/sec, the micro-sorter can readily be applied to sort rare cells.

In conventional FACS, loss of cell viability is a concern due to the high hydrodynamic forces involved in the acceleration, droplet formation, and the deceleration as cells enter the collection tubes, etc. A trypan blue exclusion test was performed to evaluate viability for unsorted cells and sorted cells by the PZT actuation. No significant loss of cell viability due to the PZT actuation relative to unsorted populations was observed (less than 3%), which proves the PZT actuation mechanism does not cause serious damage to cells as sorted cells are deflected with the fluid.

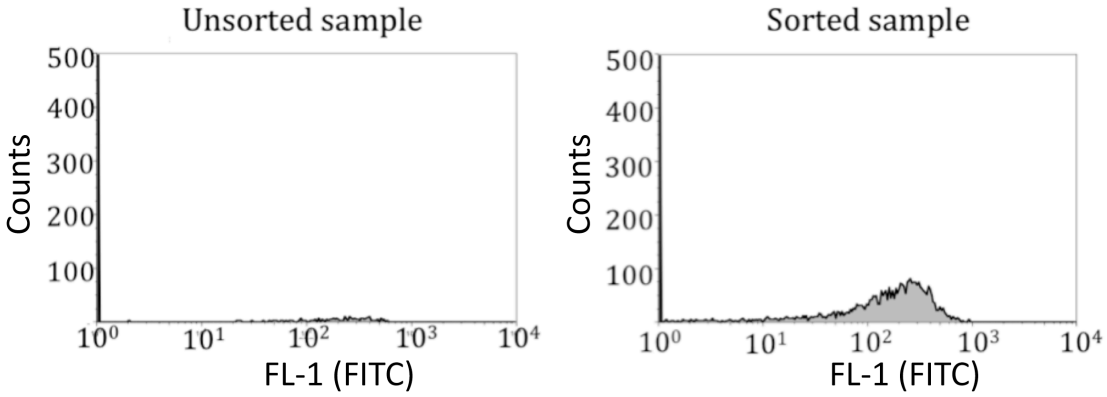

A) B)

Figure 5.9 Fluorescent intensity (FITC) histograms (gated by FSC vs SSC plots) showing the sample enrichment of K562 cells A) before and B) after sorting. The quantitative analysis yields an enrichment factor of 230 fold, which is the highest value ever reported among μFACS systems.

5.3.3 Performance comparison between μFACS and FACS

To compare the sorting performance of the integrated μFACS with one of the highest performance bench-top FACS, (MoFlo, DakoCytomation Inc., San Diego, CA),

nearly identical experimental conditions (sample concentration, initial mixture ratio, and throughput) are intentionally utilized using the bead sample (i.e. mixture of 10 μm fluorescent and 5 μm non-fluorescent beads). The result of comparison is shown in Table 1. While the MoFlow outperforms the integrated mFACS in terms of sample enriching capability, the gap is not too large considering the sophistication, size, and price ($500k) of the MoFlo system.

The μFACS system could significantly bridge this gap in sample enrichment by incorporating the capabilities of scattering parameter measurement, three-dimensional flow confinement, and the use of a narrower nozzle structure. Since the current system performs sorting based only on fluorescence, the addition of a scattering parameter can enhance purity by aborting sorting decisions whenever cells are traveling too close together. With 3-D flow confinement and a narrower nozzle structure, the effect of velocity variation in the vertical direction can be minimized, further preventing two beads from being sorted together due to velocity variations (e.g. cells catching up cells in front of them). For future work, incorporation of the FSC parameter can be achieved by integrating on-chip waveguide-lens structure [22,23] that allows in-plane optical excitation and collection. A number of 3-D confinement architectures, such as those employing the microfluidic drifting technique [24] or chevron structures [25] are compatible with the current system and can be readily integrated with the new device structure for increasing purity while maintaining high throughput operation.

Table 5.1 Summary of performance comparison between the μFACS and the MoFlo FACS

Instrument	Throughput	Initial Mixture Ratio	Final Mixture Ratio	Enrichment Factor (fold)
Integrated μFACS (beads)	1,500 beads/s	0.0067	1.34	200
Integrated μFACS (Mammalian Cells)	1,000 cells/s	0.0081	1.86	230
MoFlow (beads)	2,000 beads/s	0.0098	9.02	920

5.4 Conclusion

In this chapter, I have demonstrated, for the first time, a microfluidic μFACS with integrated piezoelectric actuator. Using a specially design spatial filter and a real-time signal processing algorithm implemented in FPGA, the system enables real-time signal amplification (~ 18 dB) and sorting event verification. These features enabled characterization of sorting efficiency, which showed a efficiency of ~84% and 0% error rate (e.g. no false positive). In addition, sample-enriching performance is characterized by sorting mixtures of bead and mammalian cell samples using the μFACS device and the performance is compared to a high-end commercial FACS. μFACS shows a enrichment factor of > 200 fold for both bead and cell samples at throughput > 1,000 cells/sec. These values are somewhat less but comparable to the values from the commercial FACS machines. However, I believe with integration of additional scattering detection functionality and 3-D flow confinement, the performance gap can be significantly bridged.

References:

[1] D. Psaltis, S. R. Quake, and C. Yang, "Developing optofluidic tech- nology through the fusion of microfluidics and optics," Nature-London, vol. 442, pp. 381–381, 2006.

[2] D. A. Chang-Yen, R. K. Eich, and B. K. Gale, "A monolithic PDMS waveguide system fabricated using soft-lithography techniques," J. Lightw. Technol., vol. 23, pp. 2088–2093, 2005.

[3] V. Lien and Y.-H. Lo,"A prealigned process of integrating optical waveguides with microfluidic devices," IEEE Photon. Technol. Lett., vol. 16, pp. 1525–1527, 2004.

[4] X. Cui, L. M. Lee, X. Heng, W. Zhong, P. W. Sternberg, D. Psaltis, and C. Yang, "Lensless high-resolution on-chip optofluidic microscopes for *Caenorhabditis elegans* and cell imaging," PNAS, vol. 105, pp. 10670-10675, 2008.

[5] S. H. Cho, J. Godin, "Optofluidic waveguides in Teflon AF-coated PDMS microfluidic channels," IEEE Photonics Technology Letters, vol. 21, pp. 1057-1059, 2009.

[5] N. Pamme and C. Wilhelm, "Continuous sorting of magnetic cells via on-chip free-flow magnetophoresis," Lab Chip, vol. 6, pp. 974-980, 2006.

[6] N. Pamme and A. Manz, "On-chip free-flow magnetophoresis: continuous flow separation of magnetic particles and agglomerates," Anal. Chem., vol. 76, pp. 7250-7256, 2004.

[7] J. Kruger, K. Singh, A. O'Neill, C. Jackson, A. Morrison, and P. O'Brien, "Development of a microfluidic device for fluorescence activated cell sorting," J. Micromech. Microeng., vol. 12, pp. 486-494.

[8] A. Wolff, I. R. Perch-Nielsen, U. D. Larsen, et al. "Integrating advanced functionality in a microfabricated high-throughput fluorescent-activated cell sorter," Lab Chip, vol. 3, pp. 22–27, 2003.

[9] J. M. Coulson, J. F. Richardson, J. R. Backhurst, J. H. Harker, Chemical Engineering, 2nd edn Butterworth-Heinemann Ltd, Oxford, pp. 970, 1982.

Chapter 5 or portion thereof has been published in ***Biomedical Microdevice,* Vol. 11, Iss. 6, pp. 1223-1231** and ***Lab Chip*, Vol. 10, pp. 1567-1573.**

Chapter 6

An integrated μFACS technology combined with Tyramide Signal Amplification enhanced Fluorescence in situ Hybridization (TSA-FISH) for isolation of rare bacteria and removal of cell-free DNA.

With advances in microbiology, it is known that the earth is inhabited by a vast diversity of microbial communities. A human alone hosts about 10^{14} microbial cells of a

wide variety of species. The complex interactions and activities of microbes in our ecosystem cannot be fully understood without dissecting their genetic materials. However, despite significant progress in microbial genomics, it is estimated only < 1% of the species have been cultured and genotyped [1]. Due to tremendous advances in genome amplification technology such as multiple displacement amplification (MDA) and DNA sequencing technology, researchers now are able to explore microbial populations without the need for cell culturing [2, 3].

Metagenomic analysis is a culture-independent approach for classifying and genotyping the diversity of environmental microbial samples. The most commonly used approach in metagenomics involves cell isolation using FACS followed by genome amplification using MDA. Even though microbes in simple communities (i.e. mixture with only a few microbial species) can be sequenced with purified bulk DNA [4], there are two key challenges in isolating and sequencing more complex environmental samples: 1) conventional target-specific FISH labeling lacks fluorescent intensity due to limited amount of microbial DNA/RNA content causing numerous microbial species from being identifiable. As a result, species that are undetectable cannot be isolated. 2) The presence of contaminating cell-free DNA in environmental samples can cause high background noise during MDA process, and this in turn can cause complications and waste of reagents during sequence assembling (e.g. erroneous sequences could be ascribed to the targeted microbe) [5, 6].

Conventionally, commercial FACS machines are often used to isolate and removal cell-free DNA, but cross contaminations from previous runs and the fact that

the instruments perform sorting in an opened system (e.g. collection tubes are open to surrounding air during sorting) could significantly limits its cell-free DNA decontaminating capability. Alternatively, various μFACS technologies that sort cells using optical [7], electroosmotic [8], dielectrophoretic [9], and hydrodynamic switching [10, 11] methods have been demonstrated, but to our knowledge, none of them has yet been applied to metagenomics that addresses the issues of cell-free DNA contamination as well as detection sensitivity for sorting rare unculturable bacteria. Thus, in this chapter, we propose an integrated μFACS technology, which not only provide significant cost (~10-100 times lower relative to FACS) and size reduction but also sort targeted microbes under closed-system operation, combined with the modified tyramide signal amplification based fluorescence in situ hybridization (TSA-FISH) to address the aforementioned challenges. In addition, we have compared the cell-free DNA removal capability between FACS and the integrated μFACS in dual round sorting showing comparable results.

6.1 Detection sensitivity enhancement

In a fluorescencen-activated cell sorting, sorting cannot be done without having sufficient detection sensitivity. Ultimately, detection sensitivity is controlled by three main factors: 1) electronics noise (e.g. noise from PMT, amplifier circuit, A/D converter), 2) noise from light scattering (from cells or side walls of the microfluidic channel), and 3) fluorescence emitted from the cells. In the current μFACS system, electronics noise is minimized by using a low-dark count PMT, low-noise amplifier

(low bandwidth), and a 16-bit A/D input module. However, improvements in the other two factors require novel engineering design and biological approach. Thus, in this section, I will demonstrate sensitivity enhancement using the modified TSA-FISH protocol for cell labeling and optofluidic liquid-liquid core waveguide with two-step light confinement.

6.1.1 TSA-FISH for flow cytomeric applications

Tyradmide Signal Amplification (TSA) utilizes the catalyltic activity of horseradish peroxidase (HRP) to increase number of binding fluorophores localized in the vicinity of the HRP-target interaction sites. TSA mechanism is first described by Bobrow et al. [12] for solid-phase assays. Commonly, researchers apply the methodology in immunohistochemistry studies [13-16] and biological samples fixed on glass slides [17]. However, the current μFACS requires samples prepared in suspension and therefore, the standard TSA-FISH protocol (from Invitrogen, Inc.) is modified for flow cytometric applications.

6.1.1.1 Modified TSA-FISH protocol

The general TSA-FISH workflow is shown in figure 6.1 where either mouse gut sample (environmental samples) and *e. coli.* could be used. In the beginning stage, *e. coli.* sample is used to validate the feasibility of the method. At first, 100 μl of *e. coli*. at concentration of 10^6 cells/μl is fixed in 100% EtOH for 1 hr. The cells are washed twice followed by labeling of biotyinated FISH probe (Invitrogen, Inc.) in the hybridization buffer (H_2O: 86 uL, 2M NaCl: 90 uL, 0.1% SDS: 20 uL, 2M Tris: 2 uL) with diluted

biotinylated probe concentration (1000 ng/uL) at 46 °C for 1.5 hrs. After pelleting the cells, the sample is incubated with 500 µl washing buffer (H_2O: 395uL, 0.1% SDS: 50uL, 2M NaCl: 45uL, 2M Tris: 5uL, 0.5M EDTA: 5uL) at 48 °C for 20 mins. The rest of the HRP and tyramide labeling reagents is purchased from Invitrogen (488 Alexa TSA kit) with a written protocol. The protocol is again slightly modified for labeling of cells in suspension. After incubation in washing buffer, the sample is incubated in diluted HRP conjugation solution (1:50 in 1 % blocking solution/PBS) on a rocking plate to ensure uniform labeling (prevent HRP/cells from sedimentation) for 6 hrs. Followed by two washing steps with PBS, the sample is incubated in tyramide working solution (1:50 in amplification buffer) for 2 hrs on a rocking plate. After incubation, the sample is washed two times using PBS solution.

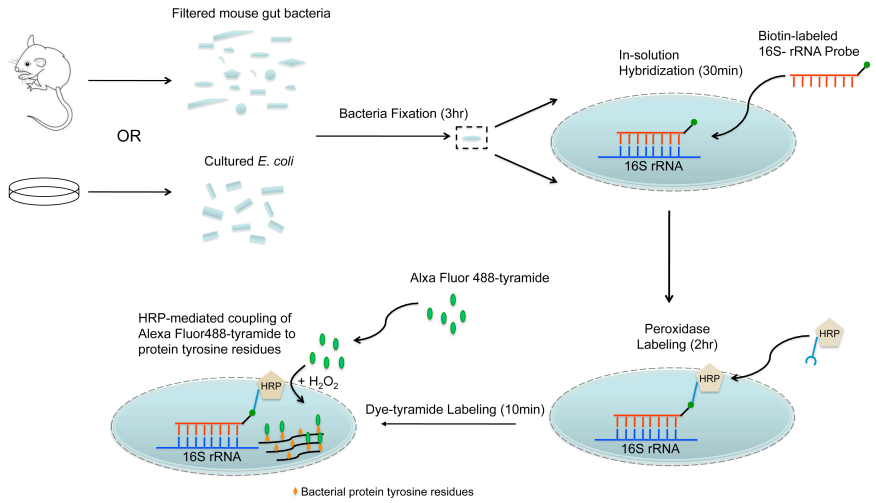

Figure 6.1 Workflow of the TSA-FISH protocol. Biotin-labeled 16S rRNA probe is used to target bacteria of interest followed by conjugation of HRP to the rRNA probe. HRP-mediated catalytic reaction activate alexa488-labeled tyramide derivatives causing localized binding of short-live tyramide radicals to tyrosine residues.

6.1.1.2 Flow cytometric analysis of TSA-FISH

To evaluate the effectiveness of the modified TSA-FISH labeling, we used *e. coli.* samples and label them with standard FISH fluoro-probes and with TSA-FISH. Figure 6.2 shows the result of the flow cytometric analysis on two standard FISH fluoro-probes (FAM and Alexa488 fluoro-probes) and TSA-FISH with alexa 488 fluoro-tyramide. Labeling with standard FISH fluoro-probes shows fluorescent signals very close to or overlap (FAM fluoro-probe) with the background noise. This is undesirable especially during fluorescence-activated sorting process since contaminating background noise could adversely affect the purity of the sorted mixtures. In addition, it is believed that a number of uncultivated bacteria could have significantly lower DNA/RNA content than the experimented *e. coli.* samples implying that undetectable bacteria using standard FISH fluoro-probes cannot be isolated and therefore cannot be sequenced. However, TSA-FISH methodology provides signal enhancement (10-30 fold over conventional FISH) that would enable more rare unculturable bacteria to be detected and genotyped by sequencing.

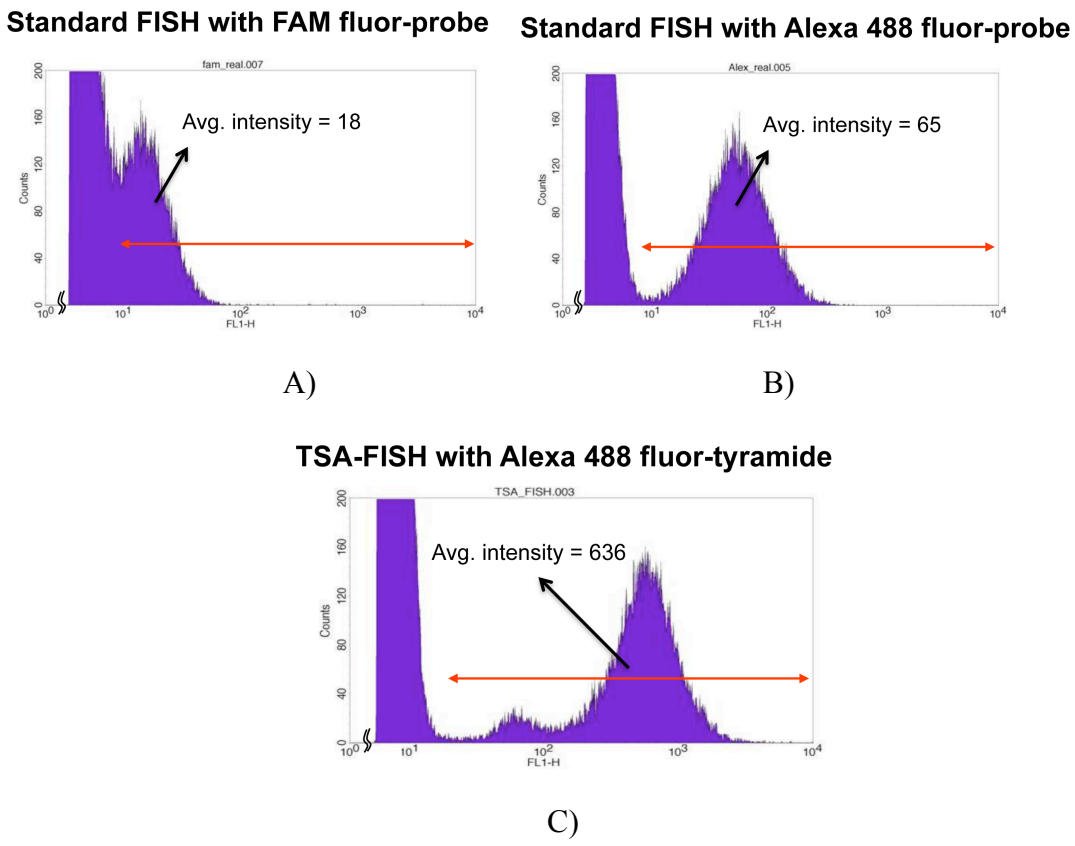

Figure 6.2 Comparison of standard FISH probe labeling with TSA-FISH on *e. coli.* samples. Fluorescent intensity histograms of standard FISH with A) FAM fluor-probe and B) Alexa 488 fluoro-probe show fluorescent intensities close to the baseline noise where as C) TSA-FISH with alexa 488 fluor-tyramide show intensities well above baseline noise. The TSA-FISH demonstrates ~ 10-30 fold enhancement over standard FISH fluoro-probes.

6.1.2 Two-step light confinement using liquid-liquid (L^2) core waveguide inside a TF AF-coated microfluidic channel

To increase laser excitation intensity and lower background light scattering, a novel two-step light confinement design is implemented. Figure 6.3A shows the two-

step light focusing mechanism. The laser light is illuminated off from the optical fiber and is first confined into the Teflon AF-coated microfluidic channel by total internal refraction (TIR). Within the microfluidic channel, another L^2 core waveguide is formed using sucrose-based solution (~13.5% sucrose in PBS). As a result, most of the light guided into the microfluidic channel is also focused into the sheath fluid-confined sucrose-based sample channel. Figure 6.3B and figure 6.3C show the signals detected off from 5.7-μm fluorescent beads (490/530 nm) under identical experimental conditions (e.g. laser intensity, flowrates, PMT settings, etc) showing an estimated SNR enhancement of ~ 14-20 dB. There are two main factors that lead to the SNR enhancement, namely increase in excitation intensity and reduction of scattering noise. Teflon-coated channel is 200-μm wide whereas the width of the sheath fluid-confined sample flow is ~ 40 μm. This suggests that there is a 5-fold increase in illumination intensity. From literature, L^2 core-cladding interface (between sheath fluid and sample flow) is known to be optically smooth [a new river of light]. Thus, by focusing light into the L^2 core sample flow, random light scattering from the microfluidic side-walls is minimized resulting in significant reduction in background noise.

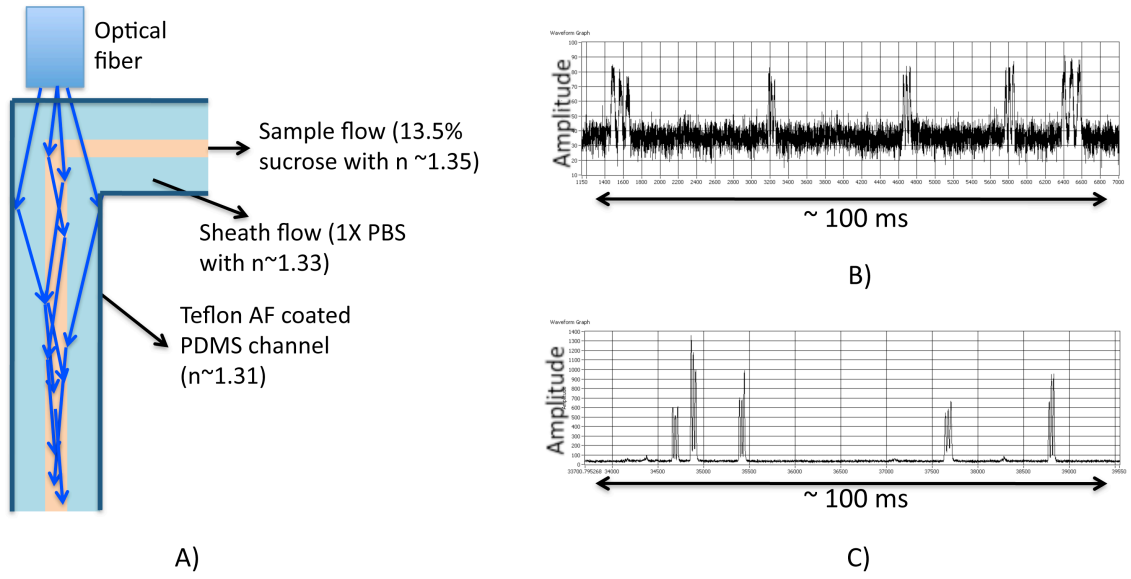

Figure 6.3 A) Schematics of optofluidic two-step light confinement showing laser illumination is first confined in TF AF-coated microfluidic channel followed by another light confinement into the sucrose-based sample flow. Detection of 5.7-μm fluorescent beads using A) only single-step light confinement (into TF-AF coated microfluidic channel) and B) two-step confinement into sucrose-based sample flow is shown above. The estimated SNR enhancement is ~ 14-20 dB.

With the sensitivity enhancement from the modified TSA-FISH and the two-step L^2 core waveguide confinement, individual *E. coli.* can be readily detected by the integrated μFACS as shown in figure 6.4A. As mentioned previously, due to the developed match-filter based amplification algorithm, the signals could be further amplified by a factor of ~ 18 dB. Figure 6.4B shows the real-time processed signals. Thus, with clear identification of individual bacteria, removal of cell-free DNA and sorting of rare bacteria become possible.

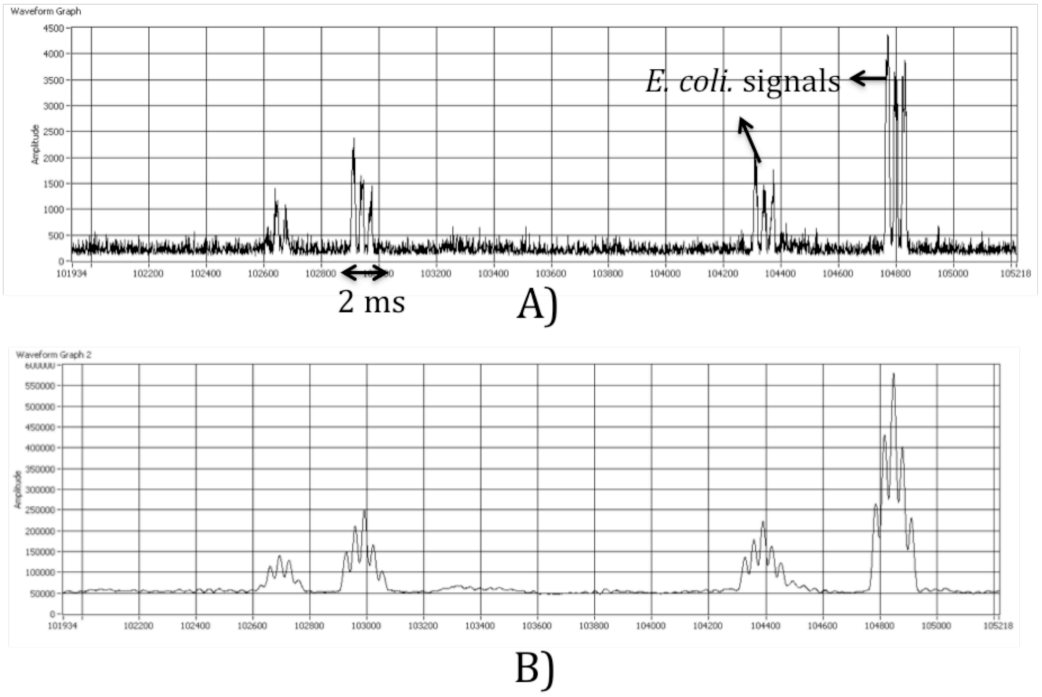

Figure 6.4 Detection of TSA-FISH labeled *e. coli.* A) Raw signals detected from individual *e. coli.* Signal modulation of detected signals enable further real-time amplification. Processed signals are shown in B) with estimated SNR enhancement of ~ 18 dB.

6.2 Cell-free DNA removal

Quantification of cell-free DNA in a given environmental sample poses a great challenge to experimentalists because we do not know where they come from (e.g. DNA from mammalian cells, bacteria, and airborne virus) and what their DNA sequences are. As a result, there is no PCR primer that allows quantification. Thus, to characterize cell-free DNA removal capability, we performed a dual-round sorting experiment on TSA-FISH labeled *E. coli.* cells with spiked in lambda phage DNA (10 ng/μl). ~100k and

10k cells are sorted for 1st and 2nd round sorting. Collected volume for each round is ~ 1.5 ml. Since commercial FACS is still the most widely used instrument for cell-free DNA removal, we performed similar experiment (~100k and 10k cells for 1st and 2nd round) on a commercial FACS (MoFlo, DakoCytomation Inc., San Diego, CA) except the collected volume is ~ 1 ml. Quantification of lambda DNA for each sorting round is done using quantitative PCR (qPCR) with lambda specific primer. Even though the collected volume is not the same, amount of lambda DNA could be readjusted by dilution factor of 1.5 (e.g. 1.5 ml for μFACS and 1 ml for FACS) after qPCR quantification.

Figure 6.5 shows the qPCR curves for each sorted mixture from both instruments. Three qPCR experiments (shown in three curves of the same color) are performed for each sorted mixture and these curves show consistent cycle number, suggesting the quantification method is repeatable and reliable. Visual comparison shows both instruments produce similar results after 1st round of sorting and commercial FACS removes slightly more lambda DNA after 2nd round. However, these results have not been adjusted for dilution factor. After dilution factor adjustment, comparison in numerical values is shown in table 6.1. Fold reduction is calculated by taking the ratio of lambda DNA content between successive rounds. Even though commercial FACS demonstrated better cell-free DNA capability, the difference is only about a factor of ~5 after 2 rounds of sorting, which is small relative to folds of reduction for each round. This suggests, if needed, researchers can more than compensate for the difference by

performing another round of sorting. Also, the gap can be further decreased by incorporating a 3-D flow-focusing module to the integrated μFACS.

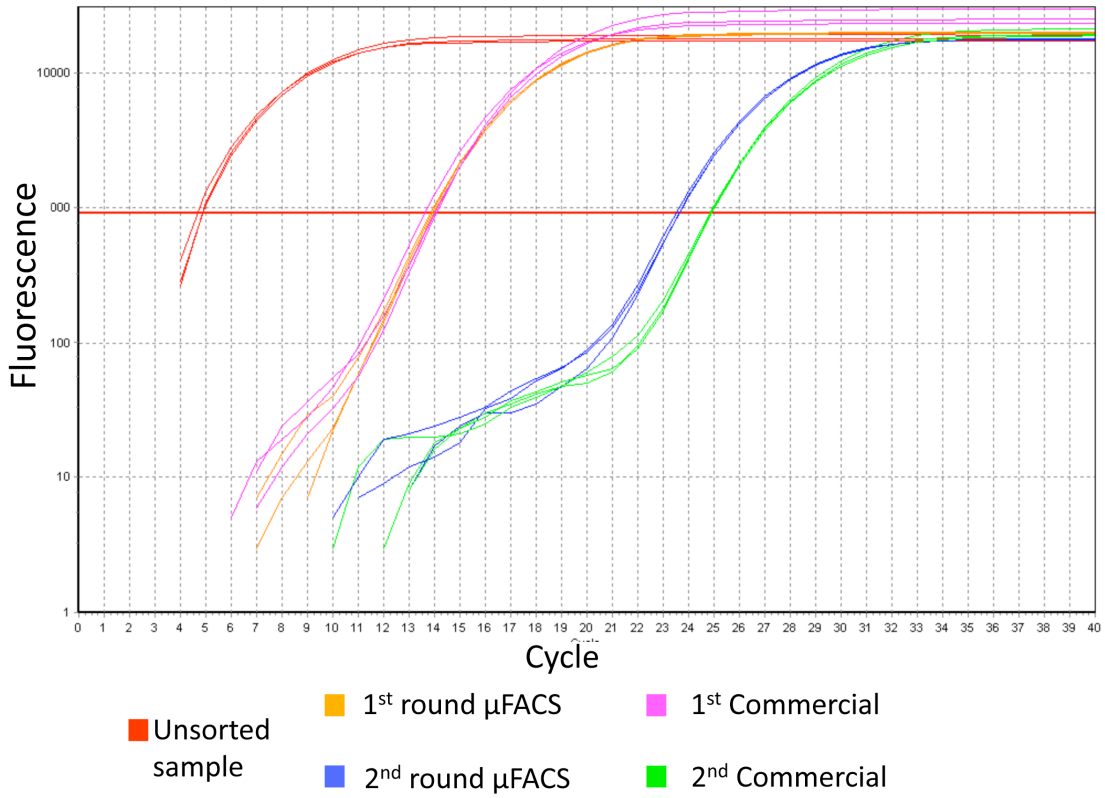

Figure 6.5 qPCR curves showing quantification of lambda DNA after successive sorting rounds. The qPCR curves (3 curves per mixture) for each sorted mixture show consistent number of cycles. From the curves, μFACS sorting yields similar result in the first round but slightly worse in the 2nd round compared to commercial FACS.

Table 6.1 Comparison of cell-free DNA removal capability between μFACS and commercial FACS

	μFACS		Commercial FACS	
Rounds of sorting	Lambda DNA (ng/μl)	Fold reduction	Lambda DNA (ng/μl)	Fold reduction
Initial amount	10	-	10	-
1st round	0.030	333*	0.014	695
2nd round	8.5×10^{-5}	351*	1.7×10^{-5}	843
Total	-	1.17×10^{5}	-	5.86×10^{5}

* The value is adjusted for a diluation factor of 1.5

6.3 Sorting of rare bacteria

Proof-of-concept demonstration of sorting of rare-abundance is performed using TSA-FISH labeled *E. coli.* The experimental methodology is depicted in figure 6.6. A mixture consisting of green and red *E. coli.* is prepared by TSA-FISH labeling with tyramides coupled to alexa-488 and alexa-647 fluorophores, respectively. A sorting strategy is implemented to enrich green (Alexa 488-conjugated tyramides) *E. coli.* from the mixture. After μFACS sorting, relative population is determined by using commercial FACS for both initial and final mixture. The enriching capabililty can be quantitatively determined by comparing the mixture ratio results.

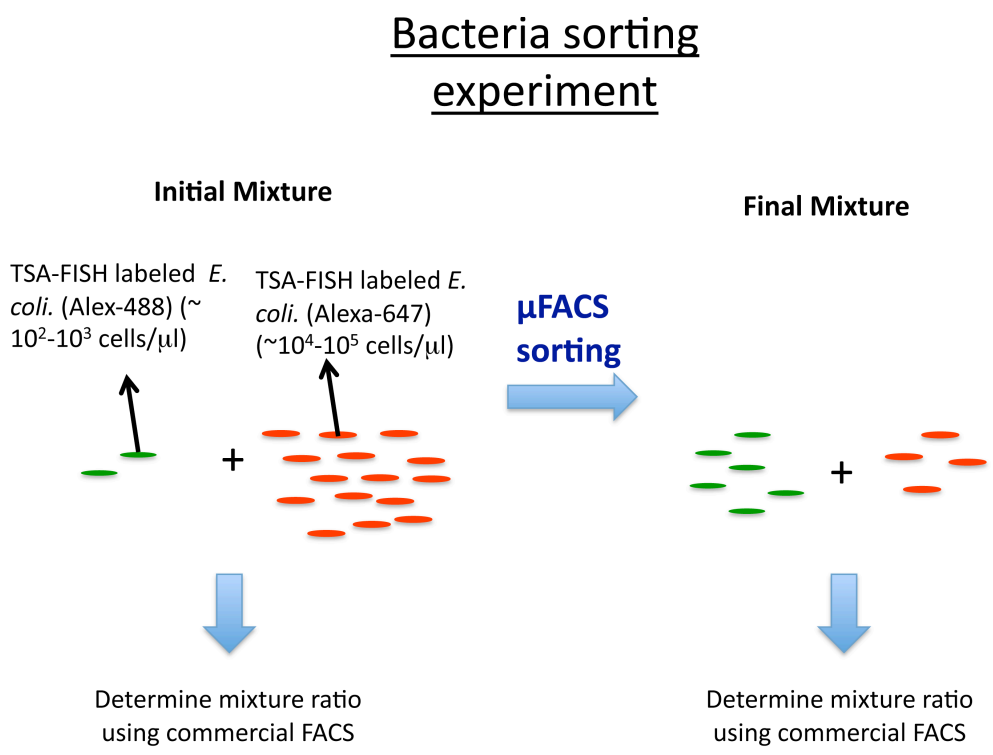

Figure 6.6 Experimental methodology in validating µFACS performance in sorting rare bacteria.

Flow cytometric analysis of the sorting result is shown in figure 6.7. After running the initial mixture through the commercial FACS, a gating strategy is determined by examing the FSC and FL-1/FL-4 (green and red) plots (figure 6.7A). By keeping the same gating conditions, we run sorted mixture through the FACS and the result is shown in figure 6.7C. The bar charts (figure 6.7B and 6.7D) show a more clear representation of sample enrichment. From the analysis, initial and sorted mixture ratios are determined as 0.0036 (1:280) and 0.79 (~ 4:5), showing an enrichment factor of ~ **223** fold. The result is very similar to the result obtained from mammalian cell sorting (230 fold). But in this experiment we have used *E. coli.* which are much smaller,

showing the versatility and consistency of the μFACS in sorting different biological samples. Moreover, with technical (two-step light confinement) and biological (TSA-FISH) improvements, we have addressed the challenge of detection sensitivity, which is a very common obstacle when dealing with small-sized biological agents.

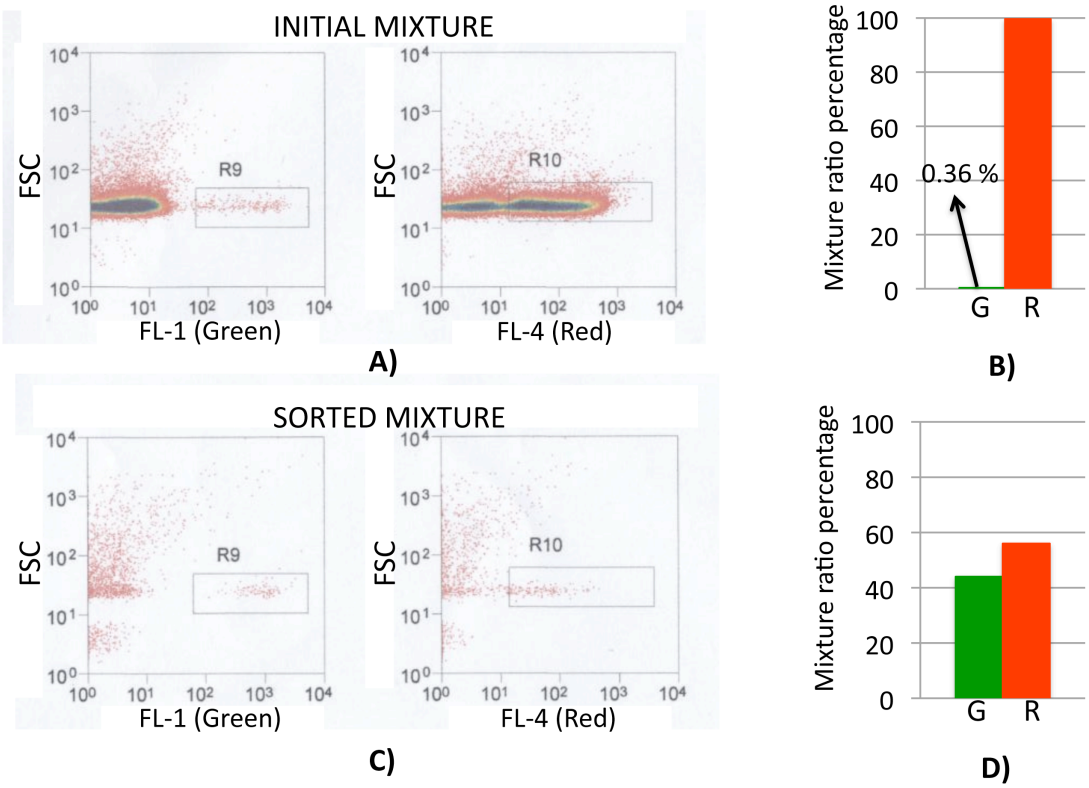

Figure 6.7 Flow cytometric analysis plots. Identical gating conditions are applied to the A) initial mixture and B) sorted mixture. The number of green and red *E. coli.* is determined by totaling the signals that are included in the gates. B) and D) show the mixture ratio percentage prior and after sorting. The analysis shows an initial and sorted mixture ratio (green:red) to be 0.0036 and 0.79, respectively, resulting in an enrichment factor of 223 fold.

6.4 Conclusion and future work

The developed TSA-FISH labeling method and the two-step light confinement L^2 waveguide significantly improve the detection sensitivity on both biological and engineering aspects. The flow cytometry-modified TSA-FISH (not only limited to μFACS system), could be applied to identify uncultivated bacteria especially bacteria that fall below the detection limit of commercial FACS. Thus, it presents a great opportunity in isolation and therefore genome sequencing of significantly more bacteria species. On the other hand, the two-step light confinement L^2 waveguide could also be implemented in other μFACS systems where sensitivity enhancement is needed. In addition to sensitivity enhancement, the integrated μFACS system has also proved the effectiveness in its bacteria sorting and cell-free DNA removal capabilities, which show comparable results relative to commercial FACS. Future work in the Human Microbiome Project (HMP) would be to isolate unculturable bacteria from environmental samples (e.g. mouse gut). Combined with microwell technologies, which are currently being developed in Prof. Kun Zhang's lab (UCSD, bioengineering department), this could provide a high-throughput pipeline in genome sequencing of unculturable bacteria.

The demonstrated performances of the μFACS serve as a major milestone in the development of a miniaturized (preferably handheld) yet low-cost μFACS that could become affordable to most research labs and clinics and perform point-of-care diagnostics in resource-poor facilities. However, even though the μFACS performances

demonstrated throughout the dissertation are shown to be comparable to FACS, the system still lacks multi-parametric capabilities (e.g. FSC and SSC) which might limit its biological applications. Thus, future work in the technical development would involve integration of multiple-parametric capabilities. One very promising work, which is currently being developed in Prof. Yu-Hwa Lo's lab, is to apply space-time coding methodology combined with arrayed waveguides to perform multi-color detection using one PMT detector. The architecture design, which is incompatible with commercial FACS, could further reduce the cost and size while enhancing the functionalities of the integrated μFACS.

References:

[1] C. S. Riesenfeld, P. D. Schloss, and J. Handelsman, "Developing optofluidic tech- nology through the fusion of microfluidics and optics," Annu. Rev. Genet., vol. 38, pp. 525–552, 2004.

[2] E. F. DeLong and D. M. Karl, "Genomic perspective in microbial oceanography", Nature, vol. 437, pp. 336–342, 2005.

[3] E. Yergeau, K. K. Newsham, D. A. Pearce, and G. A. Kowalchuk, "Patterns of bacterial diversity across a range of Antarctic terrestrial habitats," Environmental Microbiology, vol. 9, pp. 2670-2682, 2007.

[4] G. W. Tyson, J. Chapman, P. Hugenholtz et al., "Community structure and metabolism through reconstruction of microbial genomes from the environment," Nature, vol. 428, pp. 37-43, 2004.

[5] A. Raghunathan, H. R. Ferguson, C. J. Bornarth, W. Song, M. Driscoll, and R. S. Lasken, "Genomic DNA amplification from a single bacterium," Applied Environmental Microbiology, vol. 71, pp. 3342-3347, 2005.

[6] K. Zhang, A. C. Martiny, N. B. Reppas, K. W. Barry, J. Malek, S. W. Chisholm, and G. M. Church, "Sequencing genomes from single cells by polymerase cloning," Nature Biotechnology, vol. 24, pp. 680-686, 2006.

[7] M. M. Wang, E. Tu, E. R. Daniel, et al. “Microfluidic sorting of mammalian cells by optical force switching,” Nat. Biotechnol., vol. 23, pp. 83-87, 2005.

[8] A. Y. Fu, C. Spence, A. Scherer, F. H. Arnold, and S. R. Quake, “A microfabricated fluorescence-activated cell sorter,” Nat. Biotechnol., vol. 17, pp 1109-1111, 1999.

[9] D. Holmes, M. E. Sandison, N. G. Green, and H. Morgan, “On-chip high-speed sorting of micron- sized particles for high-throughput analysis,” IEEE Proceedings-Nanobiotechnology, vol. 152, pp. 129–135, 2005.

[10] J. Kruger, K. Singh, A. O’Neill, C. Jackson, A. Morrison, and P. O’Brien, “Development of a microfluidic device for fluorescence activated cell sorting,” J. Micromech. Microeng., vol. 12, pp. 486-494.

[11] A. Wolff, I. R. Perch-Nielsen, U. D. Larsen, et al. “Integrating advanced functionality in a microfabricated high-throughput fluorescent-activated cell sorter,” Lab Chip, vol. 3, pp. 22–27, 2003.

[12] M. N. Bobrow, T. D. Harris, K. J. Shaughnessy, and G. J. Litt, “Catalyzed reporter deposition, a novel method of signal amplification: application to immunoassays,” J. Immunol. Methods, vol. 125, pp. 279-285, 1989.

[13] R. d. Haas, N. P. Verwoerd, M. v. d. Corput, R. v. Gijlswijk, H. Siitari, H. J. Tanke, “The use of peroxidase-mediated deposition of biotin-tyramide in combination with time-resolved fluorescence imaging of europium chelate label in immunohistochemistry and in situ hybridization,” J. Histochem. Cytochem., vol. 44, pp. 1091-1099.

[14] H. M. Kerstens, P. J. Poddighe, and A. G. Hanselaar, “A novel in situ hybridization signal amplification method based on the deposition of biotinylated tyramine. J. Histochem. Cytochem., vol. 43, pp. 347-352.

[15] A. K. Raap, M. P. C. v. d. Corput, R. A. W. Vervenne, R. P. M. v. Gijlswijk, H. J. Tanke, and J. Wiegant, “Ultra-sensitive FISH using peroxidase-mediated deposition of biotin- or fluorochrome tyramides. Hum. Mol. Genet., vol. 4, pp. 529-534.

[16] D. Kosman, C. M. Mizutan, D. Lemons, W. G. Cox, W. McGinnis, and E. Bier, "Multiplex Detection of RNA Expression in *Drosophila* Embryos," Science, vol. 305, pp. 846, 2004.

[17] W. Manz, R. Amann, W. Ludwig, M. Wagner, and K.-H. Schleifer, “Phylogenetic oligodeoxynucleotide probes for the major subclasses of proteobacteria: problems and solutions,” Syst. Appl. Microbiol., vol. 15, pp. 593-600.